THE EFFECT OF NUCLEAR BOILING ON HEAT PIPE OPERATION

by

William Leidy Mosteller

United States
Naval Postgraduate School

THESIS

THE EFFECT OF NUCLEATE BOILING

ON HEAT PIPE OPERATION

by

William Leidy Mosteller

April 1969

THE EFFECT OF NUCLEATE BOILING

ON HEAT PIPE OPERATION

by

William Leidy Mosteller
Lieutenant, United States Navy
B.S.Ag.E., Pennsylvania State University, 1961

Submitted in partial fulfillment of the
requirements for the degree of

MASTER OF SCIENCE IN MECHANICAL ENGINEERING

from the

NAVAL POSTGRADUATE SCHOOL
April 1969

ABSTRACT

An everted experimental stainless steel heat pipe was designed and operated to observe nucleate boiling in the wick and to determine the effects of such boiling on the overall operation of the pipe. Four layers of 100 mesh stainless steel wire cloth were used as the wick structure and both water and ethyl alcohol were used as working fluids. A pressure adjusting system was included so that observations could be made as a function of internal vapor pressure.

A type of boiling was observed which did not appear to affect the overall operation of the pipe and was detectable only by visual observation. The pipe operated in a regime dominated by high liquid flow resistance. Observations indicated effective values for the pipe length, wetted wick thickness, and contact angle. With these modifications, maximum heat transfer rates were in reasonably close agreement with theory.

The pressure adjuster provided a means of easily controlling the operating conditions of the heat pipe. Heat could be removed from a constant power source at any desired temperature within the limitations of the system.

TABLE OF CONTENTS

LIST OF ILLUSTRATIONS

TABLE OF SYMBOLS

A	Pressure equation coefficient, lb_f-sec^2/ft^2-Btu^2
B	Pressure equation coefficient, lb_f-sec/ft^2-Btu
b	Wick permeability constant, dimensionless
C	Pressure equation coefficient, lb_f/ft^2
d	Effective wick thickness or wetted thickness, in
g	Local gravitational acceleration, ft/sec^2
g_o	Gravitational constant, ft/sec^2
k	Thermal conductivity, Btu/ft-hr-°F
L	Latent heat of vaporization, Btu/lb_m
M	Mesh size, wires/in
N	Working fluid parameter, Btu-hr-lb_f/ft^3-lb_m
P	Specific wetted perimeter, ft^{-1}
Q	Heat transfer rate, Btu/sec, watts
R_v	Vapor space radius, in, ft
R_v'	Effective wick radius, in, ft
R_w	Radius of wick-pipe interface, in, ft
r_c	Effective capillary radius, in, ft
r_n	Radius of bubble nucleus, in, ft
r_w	Wire radius, in
S	Wire cloth stacking factor, in/in
T	Temperature, °F
Z	Pipe length, ft
γ	Surface tension, lb_f/ft
δ	Incremental error
ε	Wick porosity, dimensionless

θ Liquid contact angle, degrees

μ Liquid viscosity, lb_f-sec/ft^2

ρ Density, lb_m/ft^3

τ Time constant, sec

ϕ Pipe inclination angle measured CCW from horizontal with the evaporator end up, degrees

Subscripts

a Axial

c Condenser

e Evaporator

ℓ Liquid

r Radial

ss Stainless steel

t Thermocouple

v Vapor or vapor space

w Wick or wall

eff Effective

max Maximum

opt Optimum

sat Saturation

ave Average

ACKNOWLEDGEMENTS

The author would like to express his appreciation to Dr. P. J. Marto of the Naval Postgraduate School for his constructive criticisms of this work as thesis advisor and to Dr. P. F. Pucci and Dr. M. D. Kelleher as departmental readers. Many thanks are due to several people whose helpful interest and technical advice contributed much toward the successful operation of the apparatus.

Also many thanks to my wife, Dana, for her patience, understanding, and valuable help in reducing the data and in typing the original copy.

I. INTRODUCTION

BACKGROUND

The heat pipe is a self-contained heat transfer device which transports heat from a hotter to a cooler portion of its structure as latent heat of vaporization and returns the condensate by capillary action. It is unique in that it can conduct large quantities of heat at nearly isothermal conditions making it many times more effective than the best homogeneous conductors. This relatively simple principle is comparatively recent in engineering technology, being first noted by R. S. Gaugler in 1942 [1] and later by D. C. Thompson in 1960 [2]. The first published report is generally credited to G. M. Grover, et al. [3].

Heat pipes have been operated from cryogenic temperatures using liquid nitrogen as the working fluid [4] up to 3600°F using a nickel pipe with silver as a working fluid [5]. The higher operating temperature pipes using liquid metals as operating fluids are generally more effective and have increasing numbers of applications in aero-space structures and nuclear power systems. Thus the majority of the research has been oriented toward these pipes using sodium, potassium, and lithium. Axial heat fluxes up to 7 KW/cm^2 have been obtained [6].

The heat transfer capability of a heat pipe is generally governed by limitations in the capillary structure. The capillary pumping limit of the wick may be exceeded so that

insufficient liquid is returned to the evaporator and this section dries out, causing failure. Also the radial heat conduction limit of the wick in the evaporator section may be exceeded causing nucleate boiling in the wick. Such boiling is generally believed to disrupt the capillary flow and also cause failure. This boiling effect does not appear to be present in the liquid metal heat pipes and consequently has not received much attention. Other investigators have noted boiling in low temperature heat pipes, usually using water as a working fluid. With the exception of A. Bähr, et al. [7] studying open channel wicks, their experiments were generally not designed to study boiling and when boiling occurred it was only observed incidentally and specific causative conditons and resultant effects were not quantitatively determined.

THESIS OBJECTIVES

The objectives of this study were to design a heat pipe in which any activity in the wick could be observed visually, to operate the pipe in such a manner that boiling occurs, and to determine the effects of such boiling on the overall operation of the heat pipe. Since boiling was expected to be related to saturation temperature and thus internal pressure, the apparatus was designed so that pressure was a controlled variable. Thus, in addition to investigating nucleate boiling, information on the effect of pressure on heat pipe operation was to be

obtained, including a workable scheme by which the pipe operating temperature could be directly controlled.

II. THEORY OF OPERATION

GENERAL

A heat pipe is a self-contained heat transfer device with no moving parts. It consists of three essential components: (1) a container, (2) a capillary structure or wick, and (3) a working fluid. The common design uses a long, slender cylinder or pipe for the container with the capillary structure adjacent to or part of the inside surface of the pipe. Figure 1 is a cutaway drawing of the typical heat pipe. When heat is added to one end some working fluid will evaporate and thus this section becomes the evaporator. Pressure difference in the vapor chamber due to this addition of vapor at the evaporator will cause vapor to flow to the opposite end. This becomes the condenser because it is cooler and vapor will condense,

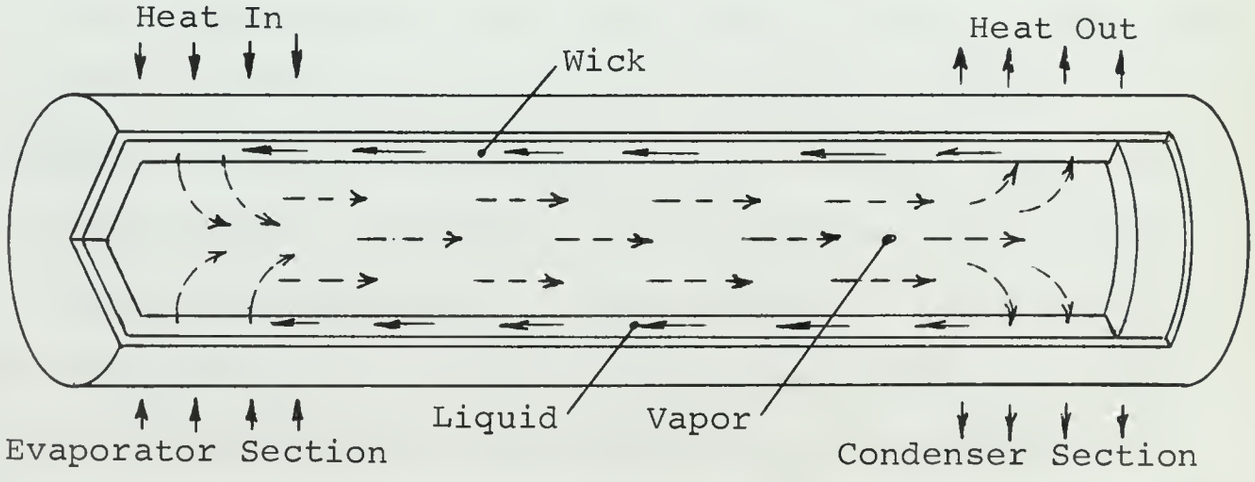

Figure 1. Cutaway View of Typical Cylindrical Heat Pipe

releasing heat which will leave the structure at this end. Condensate will return through the wick due to capillary pumping. Detailed theory of heat pipe operation is given by both T. P. Cotter [8] and B. D. Marcus [9] and a review of current theory and information is given by Cheung [6]. Only a summary of the basic theory as used in this investigation will be given here.

The necessary condition for heat pipe operation is that the capillary pumping force be equal to or greater than all the losses in the cycle. This can be expressed as

Pressure rise due to capillary forces $\geq$ Pressure drop in the liquid + Pressure head in the liquid due to gravity + Pressure drop in the vapor

And for an axial vapor flow heat pipe with a wire mesh wick this becomes [8]

$$\frac{2\gamma\cos\theta}{r_c} \geq \frac{b\mu ZQ}{2\pi(R_w^2-R_v^2)\varepsilon\rho_\ell r_c^2 L} + \frac{\rho_\ell g Z \sin\phi}{g_o} + \frac{(1-4/\pi^2)\,Q^2}{8\rho_v R_v^4 L^2} \qquad (1)$$

where Q is the axial power

r_c is the capillary radius, a wick characteristic dimension

ε is the wick porosity

b is a dimensionless constant depending upon the detailed geometry of the wick. With tortuous and interconnected pores b≈10-20

z is the pipe length

ϕ is the pipe inclination angle measured CCW from horizontal with the evaporator end up

θ is the liquid contact angle

R_w is the inner pipe radius

R_v is the vapor space radius

L is the latent heat of vaporization

γ is the surface tension

μ is the liquid viscosity

ρ_ℓ is the liquid density

and ρ_v is the vapor density

HEAT PIPE COMPONENTS

Working Fluid

The liquid, vapor, and heat transfer properties of a working fluid are important in heat pipe operation. In general, good heat pipe fluids have high surface tension, high liquid to vapor density ratio, high thermal conductivity, high latent heat of vaporization, and low viscosity. For comparison of various fluids a dimensional parameter combining some of these properties is useful [10].

$$N = \frac{\rho_\ell L \gamma}{\mu} \qquad (2)$$

It will be shown in a later section that heat transfer capability is approximately proportional to N. Some typical values of N, in Btu-hr-lb_f/ft^3-lb_m, are water at 70°F, 138; ethyl alcohol at 70°F, 9.9; and sodium at 1300°F, 1983.

Capillary Structures

The wick of a heat pipe serves two purposes, to provide a return path for the condensate and to provide

the capillary pumping indicated in the term on the left of equation (1). It is generally advantageous for the wick structure to have a thermal conductivity equal to or greater than the working fluid so that the wick will not hinder radial heat transfer. For liquids with a low thermal conductivity a metal wick improves overall conductivity and thus reduces the amount of superheat in the liquid and the possibility of boiling.

Wicks of generally homogeneous structure have been made using sintered metal fibers, sintered metal powder, packed beads, and layers of wire cloth commonly called the mesh or screen wick. All of these structures have a characteristic dimension, r_c, equivalent to the radius of a capillary tube, and which describes its capillary performance. Small values of r_c lead to increased capillary pumping ability, however homogeneous wick structures with such a characteristic generally have more resistance to the return flow of condensate. Optimization of r_c is discussed in a later section. It can be seen though that the homogeneous wick is not necessarily the most effective. The wire cloth wick is easy to construct and is widely used. For the plain weave, equal mesh, wire cloth wick the capillary radius is considered to be one-half the grid opening [11]. Thus r_c becomes

$$r_c = \frac{1}{2M} - r_w \tag{3}$$

where M is the mesh size, wires/in. and

r_w is the wire radius, in.

It has been found that higher performance is possible by providing less restrictive paths for the axial transport of the condensate but at the same time retaining the small r_c for capillary pumping. This is now commonly done by providing axial grooves in the pipe wall which are covered with wire cloth. Another means of providing additional axial flow of condensate was shown by S. Katzoff [12] whose pipe included axial tubes or arteries in addition to the regular wick.

The effective thermal conductivity of the wick and liquid combination is a factor in determining the superheat at the wick-pipe interface at a given heat flux. The heat transfer process through the wick is a complicated one made up of (1) bulk movement of the fluid which carries its own heat content, (2) conduction in each of the liquid and solid components, and (3) convective heat transfer between the liquid and solid components. The total effective conductivity is the sum of the effective conductivities of these three mechanisms. However, the first and third of these mechanisms contribute little to the total heat transfer and the second can be expressed as an average of the liquid and wick conductivities weighted on a porosity or void fraction basis [9].

$$k_{eff} = \varepsilon k_{\ell} + (1 - \varepsilon) k_w \qquad (4)$$

where k_ℓ is the liquid thermal conductivity

k_w is the wick thermal conductivity

In a wick structure made up of layers of wire cloth the actual contact area between wires is relatively small and may offer additional resistance to heat conduction. Therefore the k_w may be somewhat lower than the thermal conductivity of the wick material itself.

HEAT PIPE LIMITATIONS

Axial Heat Flux Limitations

The maximum axial heat flux density depends upon the working fluid, temperature, and wick geometry. Under given conditions, the axial heat flux may be limited by capillarity, entrainment, or sonic velocity. Entrainment occurs where the vapor flow picks up returning condensate from the wick-vapor interface and returns it to the condenser. The entrainment limit is the condition where so much condensate is removed from the wick that an insufficient amount reaches the evaporator and dryout occurs. Entrainment is closely related to wick geometry. Also the vapor in a heat pipe can theoretically reach the local velocity of sound as a limit, thus this sonic limit is another restriction on axial heat flux, although it is usually the highest of all restrictions. The entrainment and sonic limits will not be considered further since they are generally not restrictive on lower temperature heat pipes with wicks and working fluids such as those used in this study.

The capillarity limit refers to the condition where the capillary pumping term in equation (1) is insufficient to overcome the pressure drops of the other three terms. Capillarity is thus a function of the wick, the working fluid, and the compatability of the two. The wick and working fluid were discussed separately elsewhere. The wetting angle, θ, is an important parameter and is dependent on the surface conditions of the wick in addition to the fixed properties of the metal and the working fluid. Surface contamination or corrosion, even if only forming a thin film, can radically change the wettability of the wick. For many materials commonly used in heat pipes great care must be exercised to avoid contaminants in initially cleaning, assembling, and filling the pipe. Corrosion has a definite effect on the useful life of a pipe.

Radial Heat Flux Limitations

High radial heat flux causes high temperature gradients across the wick and liquid combination. This means high superheating of the liquid next to the pipe wall which may lead to boiling. Radial heat flux through the wick is given by the conduction equation for a cylindrical form.

$$\left(\frac{Q}{A}\right)_r = \frac{K_{eff}(T_w - T_v)}{R_w \ln\left(\frac{R_v}{R_w}\right)} \qquad (6)$$

The temperature at the wick surface will be considered to be the vapor saturation temperature, $T_v = T_{sat}$. To increase the radial heat flux the ratio R_w/R_v must be minimized. This means a thin wick which for a homogeneous structure would result in large axial flow resistance. Optimization of wick thickness is considered later.

The exact effect of boiling in the wick is not known but it is generally believed to be detrimental to the overall operation of the pipe. If bubbles were to form but be trapped by the wick structure they would form an insulating layer and reduce the radial heat flux from a constant temperature source, or raise the wall temperature when used with a constant heat flux source. Even if the bubbles were able to escape it is believed that they would disrupt the capillary flow and lead to dryout. The factor which will determine whether boiling will occur is the amount of superheat at the wick-wall interface, $T_w - T_{sat}$. The superheat required to initiate boiling depends on several factors, such as, the condition of the pipe surface, the presence of inert gas, and the completeness of wetting. The superheat required for nucleate boiling in a wick structure would likely be different than for pool boiling. The wick structure would contain many more nucleating sites, however if the thermal conductivity of the wick structure is greater than that of the liquid, more of the heat would be conducted to the wick surface by the metal and thus reduce the tendency to form bubbles.

Marcus [9] suggests the following relation for the critical amount of superheat:

$$T_w - T_{sat} = \frac{T_{sat}\gamma}{L\rho_v}\left[\frac{2}{r_n} - \frac{P\cos\theta}{\varepsilon}\right] \tag{7}$$

where P is the specific wetted perimeter - ft^{-1}

r_n is the radius of bubble nucleus - ft.

The $\frac{P\cos\theta}{\varepsilon}$ term is due to kinetic potential and is much smaller than the $2/r_n$ term and may be disregarded. Thus equation (7) becomes

$$T_w - T_{sat} = \frac{2\gamma T_{sat}}{L\rho_v r_n} \tag{8}$$

This could have been developed from considering the force balance on a nucleating bubble. The critical bubble radius of curvature, r_n, depends on the nature and geometry of the interface where bubbles nucleate. In the capillary structure r_n cannot exceed $r_c \sec\theta$ which would be conservative [8]. Y. Y. Hsu [13] has suggested a more sophisticated model for incipient boiling which describes a range of sizes of nucleating sites. This model is for pool boiling however and requires a knowledge of the thermal layer thickness. For a surface covered with a wick structure this thermal layer thickness approach becomes more complicated, so the simpler approach given by equation (8) will be used.

DIMENSIONAL OPTIMIZATION

Optimum Wick Thickness

In considering the axial and the radial heat flux limitations it was seen that wick thickness has opposing effects, suggesting some optimum thickness exists. For the homogeneous wick and disregarding the hydrostatic term in equation (1), Cotter finds an optimum value of R_v/R_w to be

$$\frac{R_v}{R_w} = \sqrt{\frac{2}{3}} \tag{9}$$

Optimum Capillary Radius

In the mesh wick both the capillary pressure developed and the resistance to flow depend on the characteristic capillary radius, r_c. Since capillary pressure varies inversely with r_c and flow resistance inversely with the square of r_c, again an optimum value can be found. Disregarding the hydrostatic term Cotter finds that r_c should be chosen so that the viscous contribution to the liquid pressure differential is one-half the magnitude of the capillary pressure term. For uniform heat addition and removal this becomes

$$r_c = \frac{b\mu ZQ}{4\pi(R_v^2 - R_w^2)\rho_\ell \varepsilon L\gamma \cos\theta} \tag{10}$$

And the maximum axial heat transfer is

$$Q_{max} = \frac{4\pi R_w^2 L}{3} \left[\frac{2\rho_v \rho_\ell \varepsilon \gamma^2 \cos^2\theta}{(\pi^2 - 4) b Z \mu} \right]^{1/3} \quad (11)$$

Optimum Length and Diameter

The effect of length on heat pipe performance is dependent on the pipe operating regime. When axial heat flux is limited by capillarity and liquid friction is dominating the pressure drop, then the heat flux is approximately inversely proportional to the length. For the optimum condition of equation (11) the maximum axial heat flux is inversely proportional to the cube root of length. If the liquid pressure drop were negligible such as with arteries or large grooves, then axial heat flux should be independent of length over a large range. Also in entrainment and sonic limited pipes the length will have little effect. Axial heat flux is nearly independent of diameter except for very small diameters. However for a given axial heat flux the radial heat flux is inversely proportional to diameter. Thus there is no one optimum length to diameter ratio for all heat pipes.

EFFECT OF NON-CONDENSABLE GASES

When a non-condensable gas is present in the heat pipe it will cause some changes in the overall operation. It will generally cause a frontal startup mode where initially only the evaporator heats up uniformly. As vapor pressure

increases, the non-condensable gas is swept out of the evaporator region until pressure in the vapor and gas are equal and a rather well-defined interface is formed between the two. As the vapor pressure increases with further increase in temperature, the vapor zone increases in length, sweeping the non-condensable gas before it and compressing it into the cold condenser end of the pipe. Thus the effective length of the condenser is reduced and the capacity of the heat pipe may be limited. However, since the vapor and non-condensable gas separate, it is possible to connect control and measuring systems to the condenser end using the non-condensable gas as a working medium which will be at a lower temperature than the vapor.

III. DESIGN OF APPARATUS

THE EVERTED HEAT PIPE

The overall design of the heat pipe used in this study was largely influenced by the requirement to observe the wick visually. A conventional wick and pipe geometry were also desirable so that results could be compared with other heat pipes. This led to the everted heat pipe design which is essentially the conventional cylindrical heat pipe of Figure 1 but built inside-out. That is, viewing from the centerline outward the components are (1) heat addition and removal devices, (2) the pipe wall, (3) the wick, (4) the vapor space, and (5) the glass containing envelope. Figure 2 is a sectional view of the everted heat pipe and Figure 3 is a photograph of the actual device.

Advantages of this design are that the entire wick is visible and problems associated with measuring heat fluxes into and out of the pipe are eliminated. The heater is inside the pipe so all electrical power delivered to the heater goes into the pipe with negligible losses. Likewise all heat removed by the condenser comes from the pipe. No attempt was made to design this pipe for optimum heat transfer or to derive the theoretical relations for this geometry. It was proportioned similar to a typical cylindrical pipe, but everted.

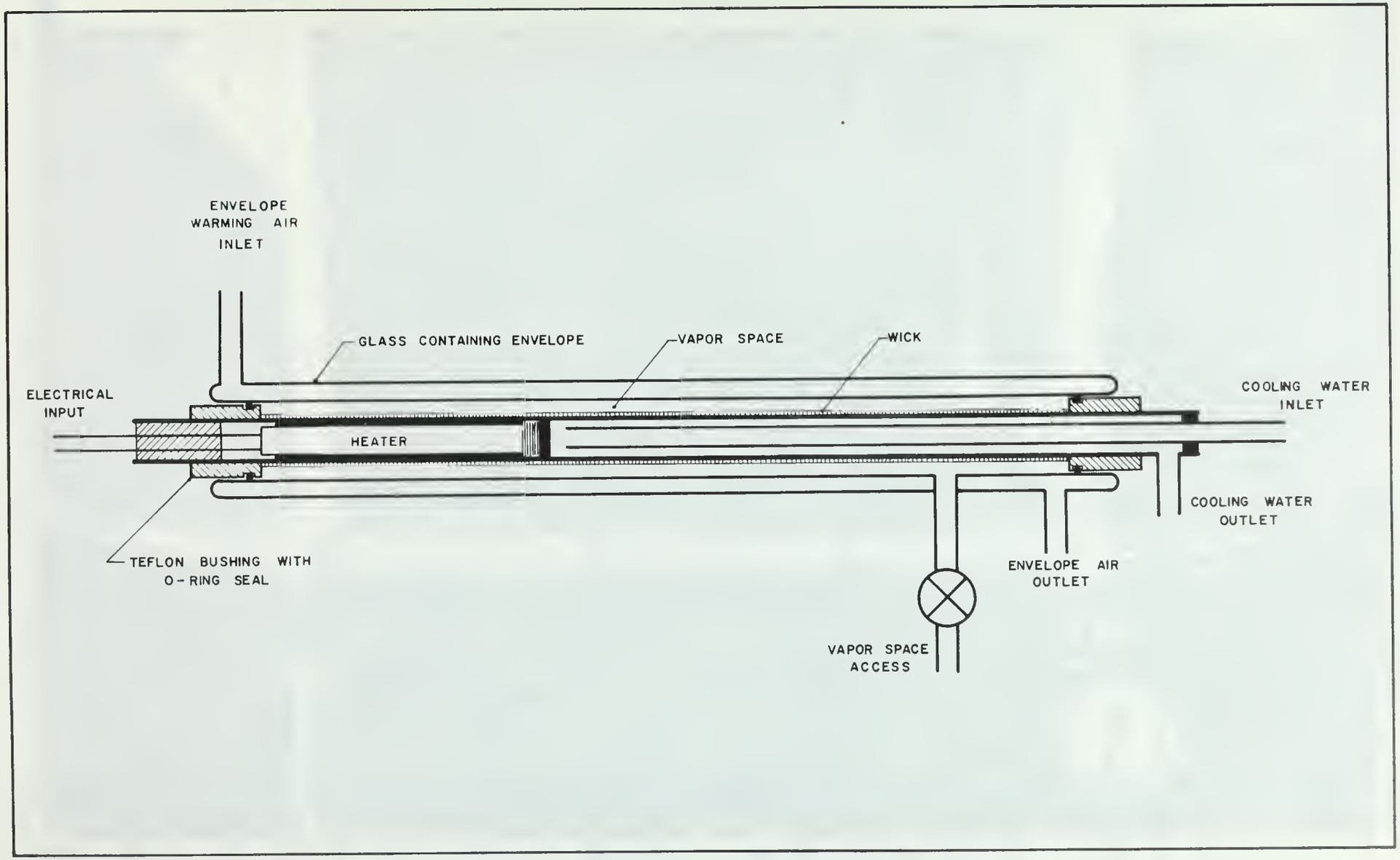

Figure 2. Sectional View of Everted Heat Pipe

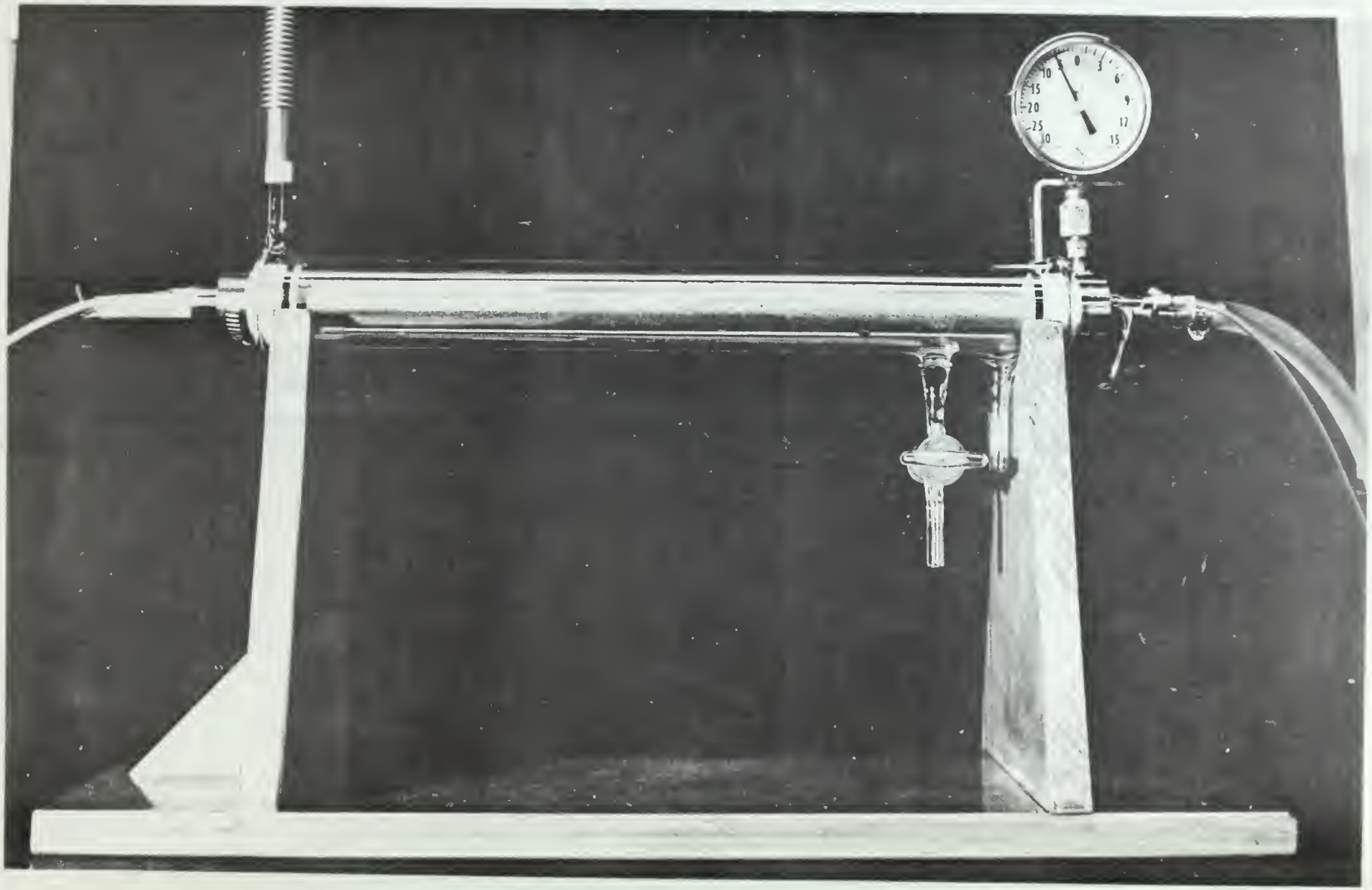

Figure 3. Photograph of Everted Heat Pipe

This design was developed independent of other studies although it is noted that Bähr, et al. [7], used a somewhat similar design in Europe in 1968. There appears to be some basic differences in their design in that the heater and condenser are different, the wick was the open rectangular channel design, and the pipe was operated vertically with the condenser above the heater.

The actual pipe used was 304 stainless steel seamless tubing with 0.750" O.D. and 0.620" I.D. The working length of the pipe was 14.0" with 4.5" for the evaporator, a 0.5" adiabatic section, and 9.0" for the condenser. Thus the length to diameter ratio, Z/D_w, is 18.7 and the condenser to evaporator length ratio, Z_c/Z_e, is 2.0. These are typical proportions used in other heat pipes.

A cartridge heater 0.500" in diameter and 4.5" long was used. A copper sleeve was used between the heater and the inside of the pipe to provide a uniform temperature distribution. This sleeve was made with a slight interference fit, shrunk with liquid nitrogen and inserted in position, thus insuring good contact with the pipe. The inner diameter of the sleeve was made with a close-sliding fit to the heater. The heater was coated with milk of magnesia before installing in the copper sleeve to prevent sticking.

The copper sleeve was 4.25" long thus giving an area of 10.01 square inches at the pipe-wick interface. This was considered the evaporator area in computing radial

heat flux. The heater was rated at 500 watts at 115 volts, however if necessary it was planned to operate this heater up to 1300 watts for brief periods by increasing the voltage. This would give a radial heat flux of 130 watts/in^2 (~20 watts/cm^2) which is the flux reported to produce boiling in an open channel wick [7]. If the heat pipe functions properly it should remove the heat adequately from the heater and keep the temperature down within normal operating limits, so this occasional overload should be tolerable. A high temperature cutout system, described later, was used in case of pipe failure and excessive temperature rise.

A 0.35" section of asbestos paper discs was placed axially between the heater and condenser as insulation. This section constituted the short adiabatic portion of the pipe. The condenser is a return flow annular design with the cooling water entering the center tube and removing heat from the heat pipe as it passes back through the annulus. An effort was made to overdesign the condenser so that it could handle any loads imposed upon it while studying conditions in the evaporator section.

The wick was made of four layers of 100 mesh plain weave, market grade, stainless steel wire cloth. The wire diameter was 0.0045". Equation (9) suggests a wick thickness of eight or nine layers, however only four were used since other pipes have successfully used two or three, and also since more layers would make it difficult to

observe bubble activity down in the wick. With water as a working fluid at 15.0" Hg vacuum and taking $\frac{b}{\epsilon} = 20$ [11] the optimum r_c from equation (10) is 0.0087". This would require four layers of 35 mesh market grade wire cloth. The maximum heat transfer under these optimum conditions was 4800 watts from equation (11). The 100 mesh size was used because of its wide use in other pipes rather than to attempt optimization. The wick was installed on the pipe by first tack welding one end to the pipe, then wrapping the wire cloth tightly onto the pipe for the number of layers desired and finally tack welding the remaining end.

The glass containing envelope was specially made for this apparatus and consisted of two concentric heat resistant glass tubes joined at the ends so as to enclose the annular space between tubes. The inner diameter of the envelope was 1.34" and chosen so the vapor space volume was approximately equal to the cavity volume of the similar conventional heat pipe. Some additional allowance was made for whatever boundary layer effects the glass wall may cause that would not be present at the centerline of the similar pipe. The envelope annular space between glass tubes was 0.16" and this space was originally evacuated to provide thermal insulation to the pipe. On the first everted pipe tested it was found that this vacuum enclosure did not provide sufficient insulation

to prevent condensation on the inside of the glass in the vapor space. This was corrected by pumping air through the annular space and controlling the air temperature to eliminate condensation. This air temperature was kept approximately the same as the vapor temperature to minimize heat transfer between the vapor space and the glass envelope air flow.

The pipe and glass envelope were connected at each end by teflon, TFE, bushings. Teflon was used because of its low thermal conductivity, relatively high heat resistance, and good machineability. The seal between the teflon and glass was made with a rubber O-ring covered with high vacuum silicon grease. The seal between the teflon and the pipe was made by compressing the bushing with a hose clamp. Pressure tap and thermocouple feed-throughs were made through the bushing at the condenser end. Minor vacuum leaks between the pipe and bushing and feed-throughs and the bushing were sealed with GEVAC vacuum sealer.

With the everted heat pipe in a horizontal position any liquid which condenses on the containing envelope or is expelled from the wick will collect in the bottom of the envelope. An auxiliary wick consisting of a piece of fiberglas cloth tape was placed in the evaporator end so that this free condensate could return to the main wick. This then provided an additional path for delivering liquid to the evaporator. The excess condensate in the pipe was enough to wet just half of the bottom length of the envelope.

It was therefore possible to have this excess pool either touch the auxiliary wick or not, as desired. This permitted operating the pipe with and without the extra condensate return path.

Since the wettability of stainless steel is greatly affected by surface contamination, proper cleaning during assembly was important. The wick was cleaned in an ultrasonic cleaner using a commercial cleaning compound. The pipe was also cleaned thoroughly with this cleanser. Both the pipe and wick then received several rinses with distilled water, then acetone, followed by more distilled water. The wick was then assembled on the pipe with all handling done with clean rubber gloves until the containing envelope was in place. This method seemed satisfactory for a new wick. It was also tried on an assembled wick which had been in use. This wick appeared contaminated and had poor wettability with water. The above procedure did not improve wettability appreciably so a dilute solution of sulfuric acid was used, followed by distilled water and acetone rinses. This did clean the contaminated wick giving marked improvement in wettability and also a bright, clean appearance.

The amount of working fluid in a heat pipe is fairly critical. There should be enough to completely fill the wick with liquid and the space with vapor under the highest operating conditions of the pipe. Marked detrimental effects can be expected if the amount deviates outside a

95% to 110% range of the correct value. With this heat pipe there is more room for an excess so the designed amount was 120% of the exact value. Thus 18 ml was used in this apparatus. If the pipe were evacuated after the fluid was added, some of the fluid would be pumped out as vapor and lost. To avoid this the following filling procedure was used. The dry pipe was evacuated and the vacuum stopcock on the envelope closed. The 18 ml of distilled water was frozen in an Erlenmeyer flask and the flask connected to the pipe stopcock. The flask was then evacuated, the valve to the pump closed, and the flask heated to melt the ice. The pipe stopcock was opened and the flask tipped to pour the water into the pipe.

AUXILIARY COMPONENTS

Pressure Adjuster

Since it was desired to operate the pipe at different saturation temperatures it was necessary to vary the pressure. This was done by allowing a certain amount of non-condensable gas (air) in the pipe and providing a means of varying the volume. This was the function of the pressure adjuster which could provide a volume change of 24.0 cubic inches. It was a piston and cylinder arrangement with the piston position set by a lead screw and hand crank. The cylinder was a plexiglas tube, 2.475" I.D. and with piston travel from 0 to 5.0". The piston was also plexiglas and fitted with two $\frac{3}{16}$" thick O-rings as

piston rings. High vacuum silicon grease was used to improve sealing and reduce wall friction. The pressure adjuster can be seen in Figure 6.

High Temperature Cut-Out Controller

A controller on the heater circuit was provided for safety to interrupt the heater if the temperature increased above a preset level. The circuit consisted mainly of a silicon-controlled-switch (SCS) in a D.C. circuit, controlled by a thermistor placed in the cavity near the heater. When a high temperature causes the thermister to turn on the SCS, a relay will open interrupting the heater circuit. Once the SCS has been switched on in a D.C. circuit it will remain on until reset. Thus if a pipe failure occurs, the controller will activate and there will be no more power to the heater until the controller is manually reset. This should prevent damage to the apparatus due to excess heat, in the event of a dryout failure. Figure 4 is a schematic diagram of the controller.

Condenser Coolant Control

Condenser cooling water was provided from the water system with pressure being regulated by two pressure regulators. A flow rotameter was used to measure the flow rate which was held reasonably constant during operation of the pipe.

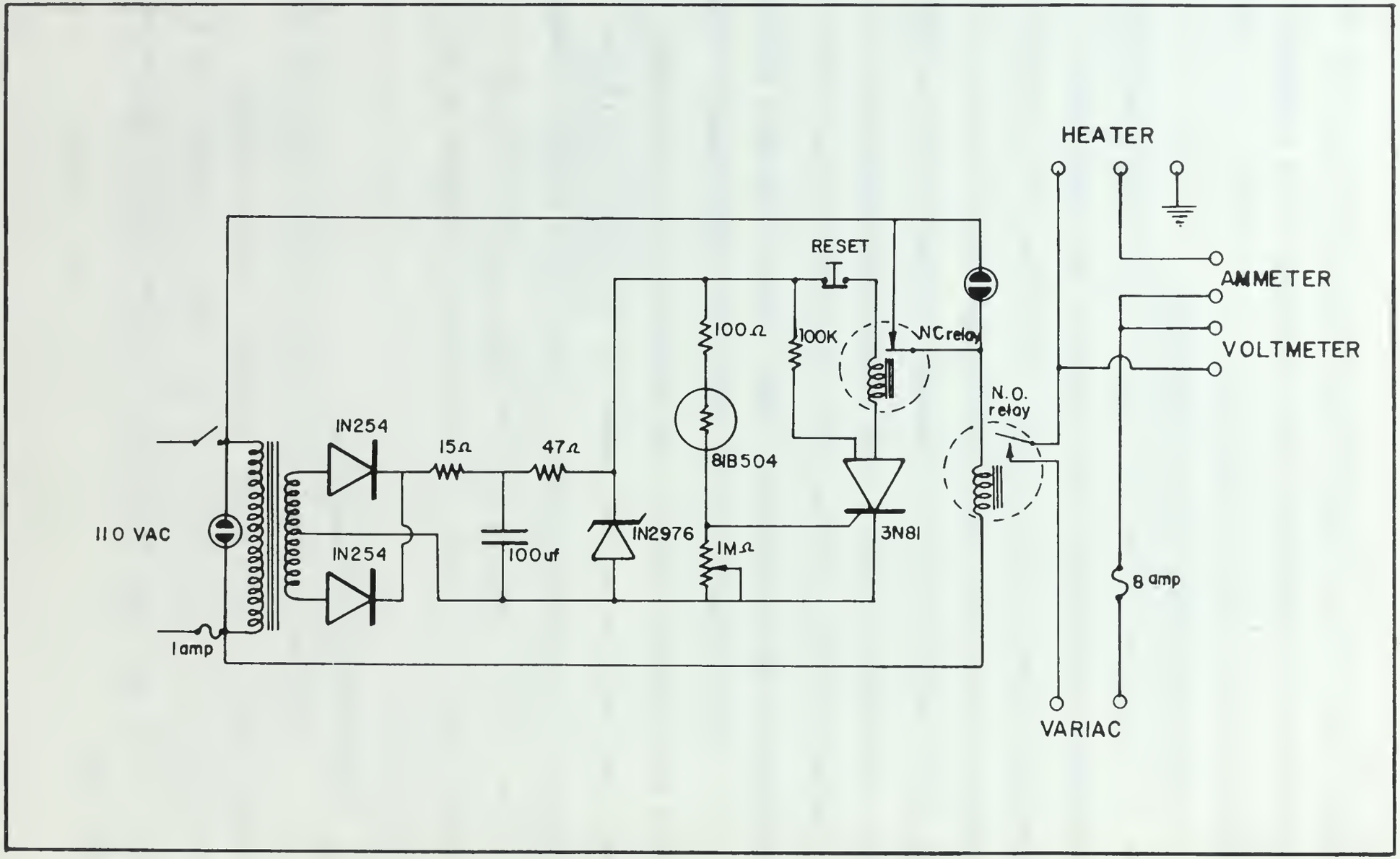

Figure 4. Schematic Diagram of High Temperature Cut-Out Coltroller

Containing Envelope Air System

An air source with no oil was necessary as oil would tend to remain in the envelope and block the view toward the wick. A diaphragm-type air compressor was used for this purpose. The air was put through a small chamber containing an electric heater where it was warmed to the desired temperature. The heater was controlled by a variac.

INSTRUMENTATION

Temperature measurements were made with copper-constantan thermocouples using a distilled water-ice bath as a reference. A total of thirteen thermocouples was used with selection being made with a thermocouple selector switch. This switch and multi-connector plug were installed in a tightly closed, insulated metal box to keep all the connecting junctions at a uniform temperature and thus reduce errors from connecting junctions. Thermocouple output was measured with a Hewlett-Packard 2010 C Data Acquisition System containing an integrating digital voltmeter and guarded data amplifier. This instrument gave a printed digital output with an accuracy of ± 0.5 microvolts.

It was desired to measure the temperature of the pipe-wick interface directly. The first pipe built had thermocouples with the junctions soldered in small cavities in the pipe surface. These thermocouples were made of 0.003" diameter wire with thin teflon insulation giving a

total diameter of 0.004" per wire. Since these wires were about the same size as the wire of the wick structure they fit between the layers of mesh cloth with no adverse geometrical discontinuities. However it was found that with the temperatures accompanying an early wick dryout the teflon insulation melted causing thermocouple failure. This approach was then abandoned.

The successful approach was to implant metallic sheathed thermocouples in the pipe surface. Six such grounded junction thermocouples with a sheath diameter of 0.031" were placed in milled axial and circumferential grooves.

The circumferential parts of the grooves were necessary to get the junctions on the top or bottom surface, however they were also beneficial in reducing the thermocouple conduction error. The sheaths were silver soldered in place and the pipe surface was machined to its original shape and polished. The junctions were then approximately one half the sheath diameter from the surface and for the radial heat fluxes encountered gave temperatures within 0.03° to 0.25° F of the surface temperature. The sheathed thermocouples were type T with special tolerance limits giving temperatures to ± 0.75° F for the range in which they were used. With these surface measuring thermocouples an integral part of the pipe it was much easier to install the wick and also facilitate changing the wick for future studies.

Four thermocouples were placed in the top surface of the pipe with two in the evaporator and two in the condenser. Two more were placed in the bottom surface of the evaporator, opposite to the two on the top. Two plain junction wire thermocouples were also placed in the vapor space. Other thermocouples were used to measure condenser inlet and outlet temperatures, envelope air temperature and the heater space temperature.

Other instrumentation included a bourdon tube combination vacuum-pressure gage which was used to measure pipe pressure. A thermocouple vacuum gage was used when initially evacuating the pipe and checking for vacuum leaks. The electrical power into the heater was measured with an AC wattmeter.

Figure 5 is a schematic representation of all components in the apparatus and Figure 6 is a photograph of the apparatus.

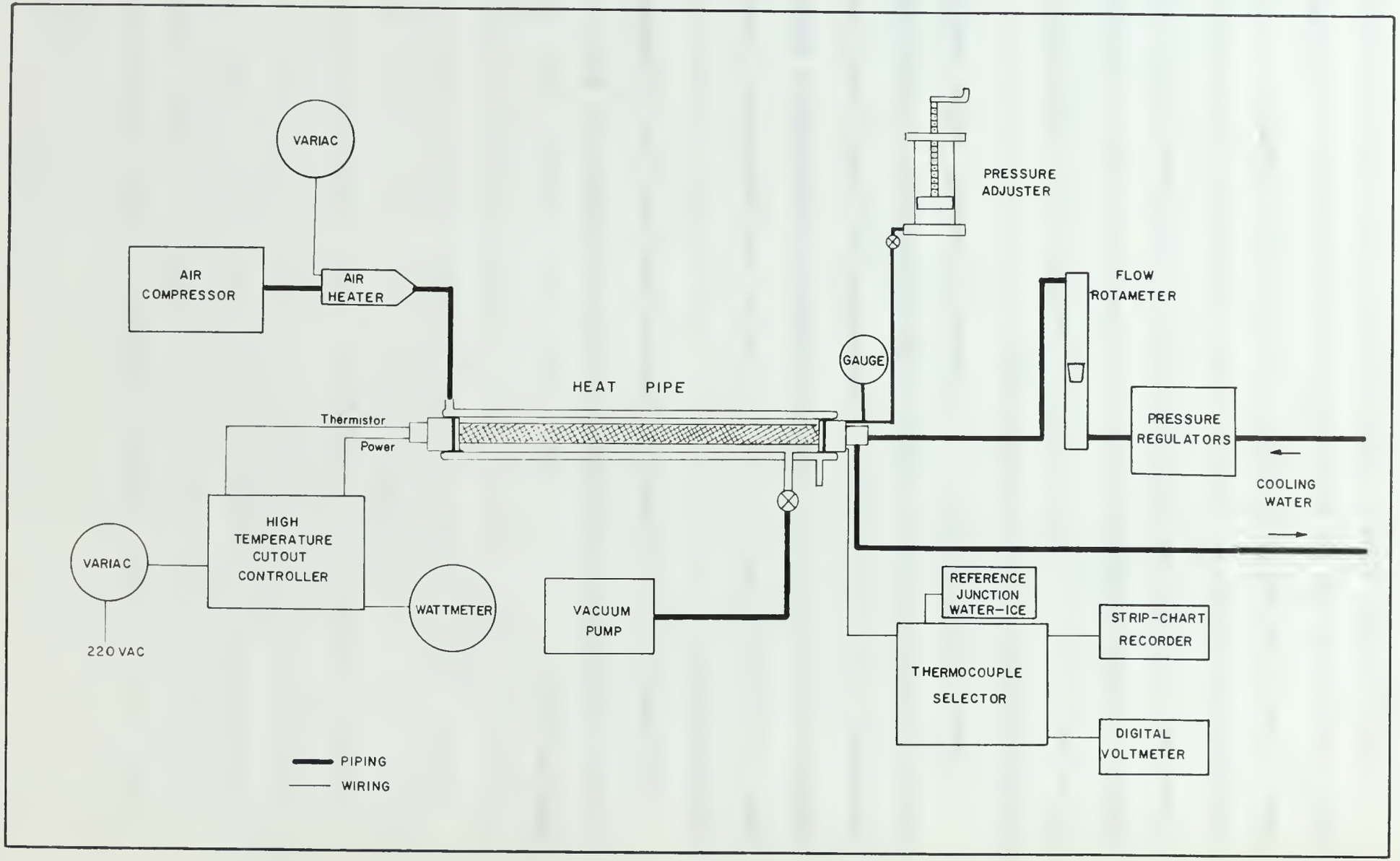

Figure 5. Block Diagram of Heat Pipe Apparatus

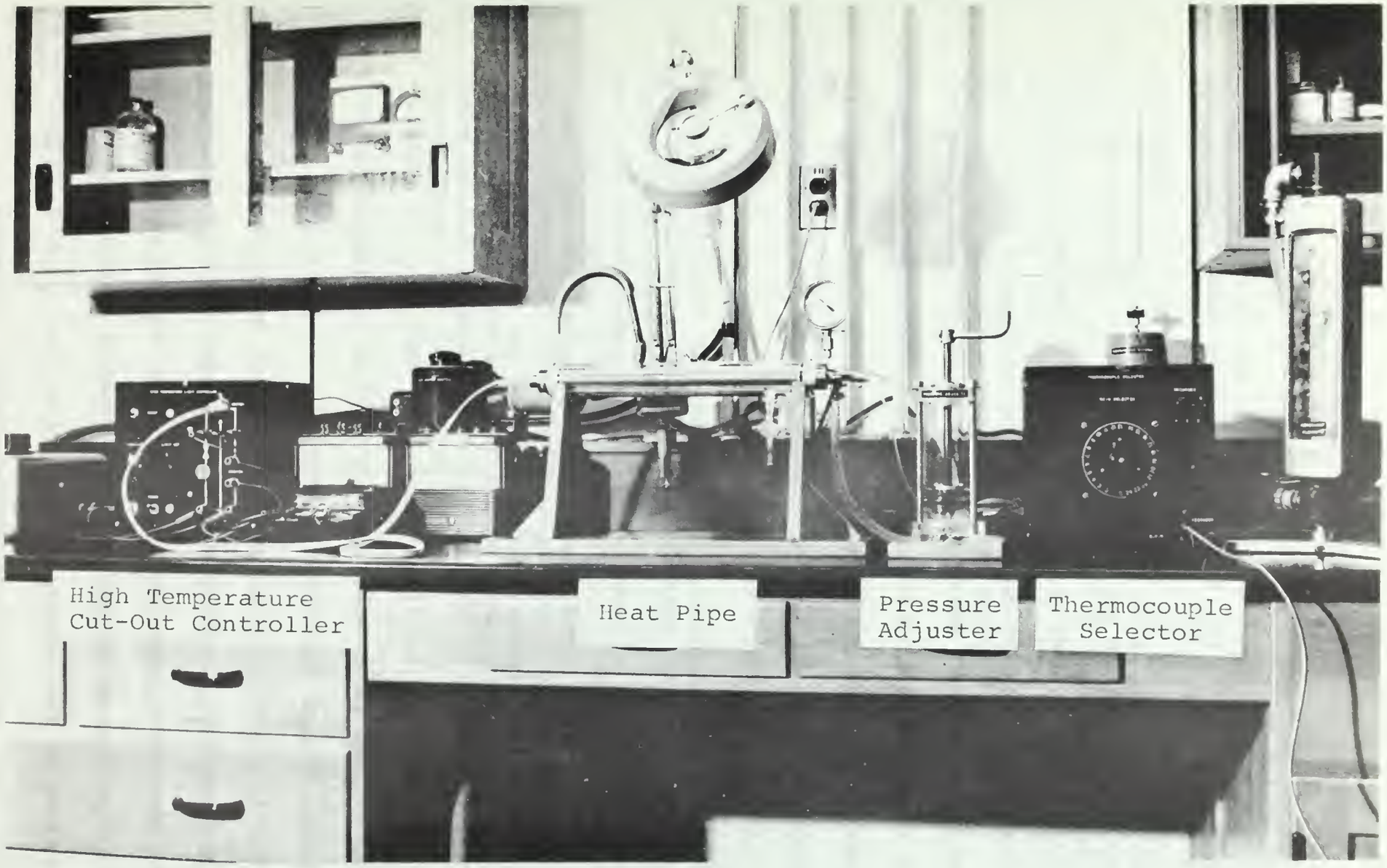

Figure 6. Photograph of Heat Pipe Apparatus

IV. EXPERIMENTAL PROCEDURE

INITIAL START-UP

When the heat pipe was first filled with water there was some difficulty in getting the wick to fill properly. By supplying coolant to the condenser and warming the glass enclosing envelope with hot air some of the working fluid vaporized and then condensed on the condenser wick. Also by shaking the pipe some of the free condensate splashed on the wick and was absorbed. A low heat input was applied until the wick became fully wet and commenced operating properly as noted by uniform temperatures in the evaporator.

NORMAL OPERATION

In preparing to operate the apparatus, first the digital voltmeter was allowed to warm up, preferably for over an hour to insure good stability. Crushed ice was then added to the reference junction dewar so that the dewar was full of ice with the interstitial spaces filled with distilled water. Readings were then made on all thermocouples to insure proper operation. In activating the heat pipe, first the condenser coolant flow was started, then the hot air flow to the envelope. When the envelope was warm the pipe heater was then energized and the pipe would commence operating. Temperature data was taken by turning the thermocouple selector switch through the range of applicable thermocouples and recording each reading with the data acquisition system output printer.

CONDENSER OPERATION

The effect of condenser flow rate on pipe operation was determined by making observations with a constant power input and varying condenser flow rate from 0.35 to 2.8 gallons per minute. The flow rate had no noticeable effect from 1.5 to 2.8 gallons per minute so in the remaining runs the flow rate was maintained at about 2.1 gallons per minute and this parameter considered constant.

CONTAINING ENVELOPE AIR CONTROL

It was desirable to keep the glass envelope free of condensate so that the wick could be observed under all conditions. It was also desirable to have no radial heat transfer between the containing envelope and the pipe. A thermocouple was placed in the air jacket nearly opposite the vapor space thermocouple. The air supply heater was then adjusted so that condensate was evaporated from the glass and the warming air temperature and measured vapor temperature were nearly equal.

CONSTANT PRESSURE DATA

To make runs at a constant pressure it was necessary to change the volume of the pressure adjuster with each increase in heat input. The strip chart recorder was used to read one of the evaporator thermocouples to monitor pipe performance while making adjustments to the system.

OTHER OBSERVATIONS

Other observations included operating the pipe at small angles from the horizontal and also using ethyl alcohol as the working fluid. The heat pipe response to change in pressure was observed by operating the pressure adjuster through a wide range of pressures.

V. DISCUSSION OF RESULTS

GENERAL OBSERVATIONS OF APPARATUS

Nature of Dryout

The upper limit of heat flux was determined by dryout in the evaporator wick. Dryout was a result of insufficient condensate being delivered by the wick to the evaporator end, thus the pipe was capillary limited. With sufficient condensate supplied to the evaporator, the evaporator temperatures were very nearly uniform. With increases in power input the pressure would also increase because of the additional vapor being added. As heat flux was increased to its upper limit insufficient liquid would reach the far end of the evaporator and temperatures there would increase. This axial temperature gradient in the evaporator was generally the first indication of approaching dryout. For a small range of heat fluxes the pipe could reach a steady operating condition with this temperature gradient.

With a further increase in power input the pipe would commence drying out. This could be noted by the evaporator temperatures increasing steadily with time. The far end of the evaporator became completely dried out and the dryout line slowly advanced down the evaporator. As this line passed a thermocouple the sharp increase in rate of temperature rise was noted, as in the strip chart recording shown in Figure 7. In this latter stage of

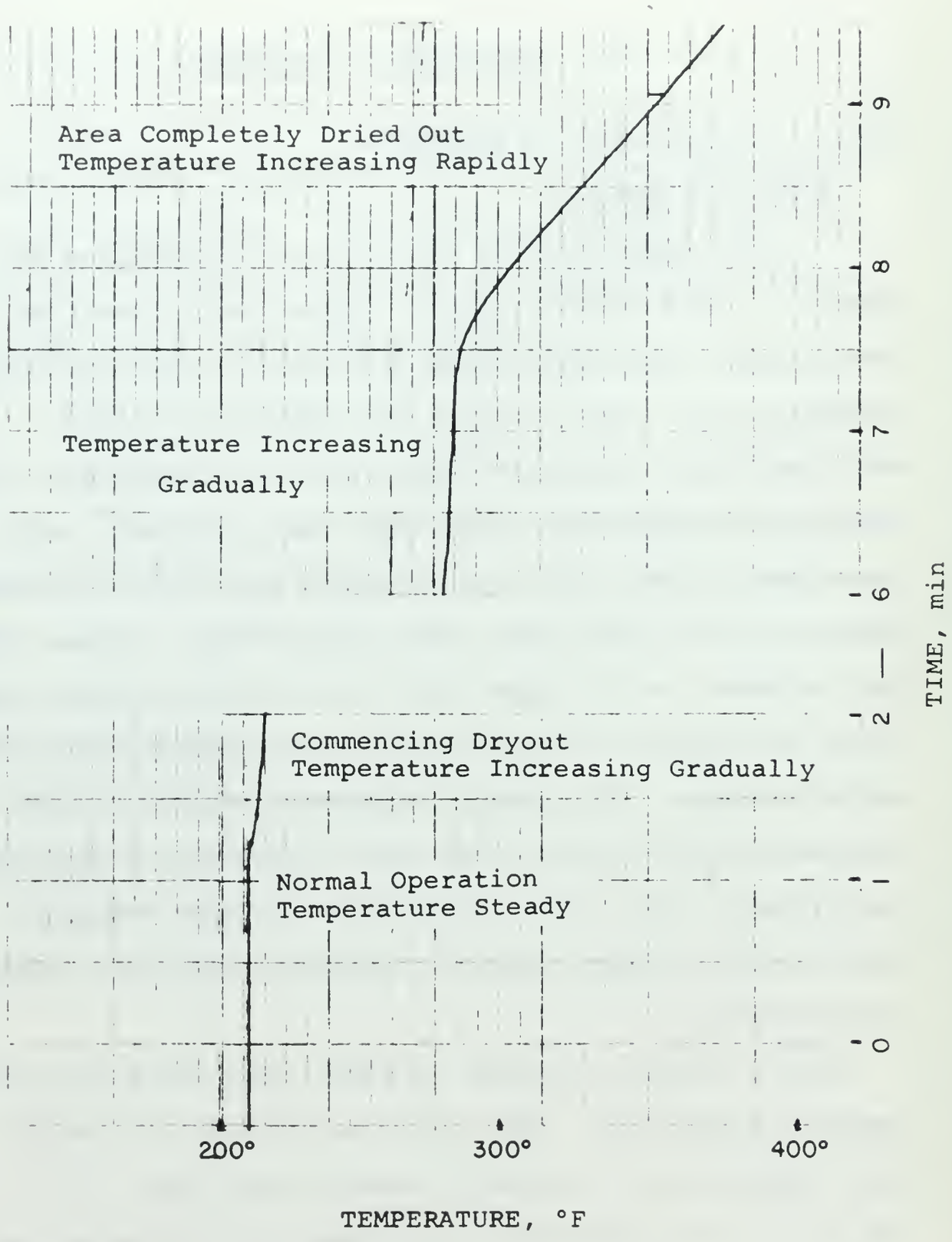

Figure 7. Strip Chart Recording of Dryout

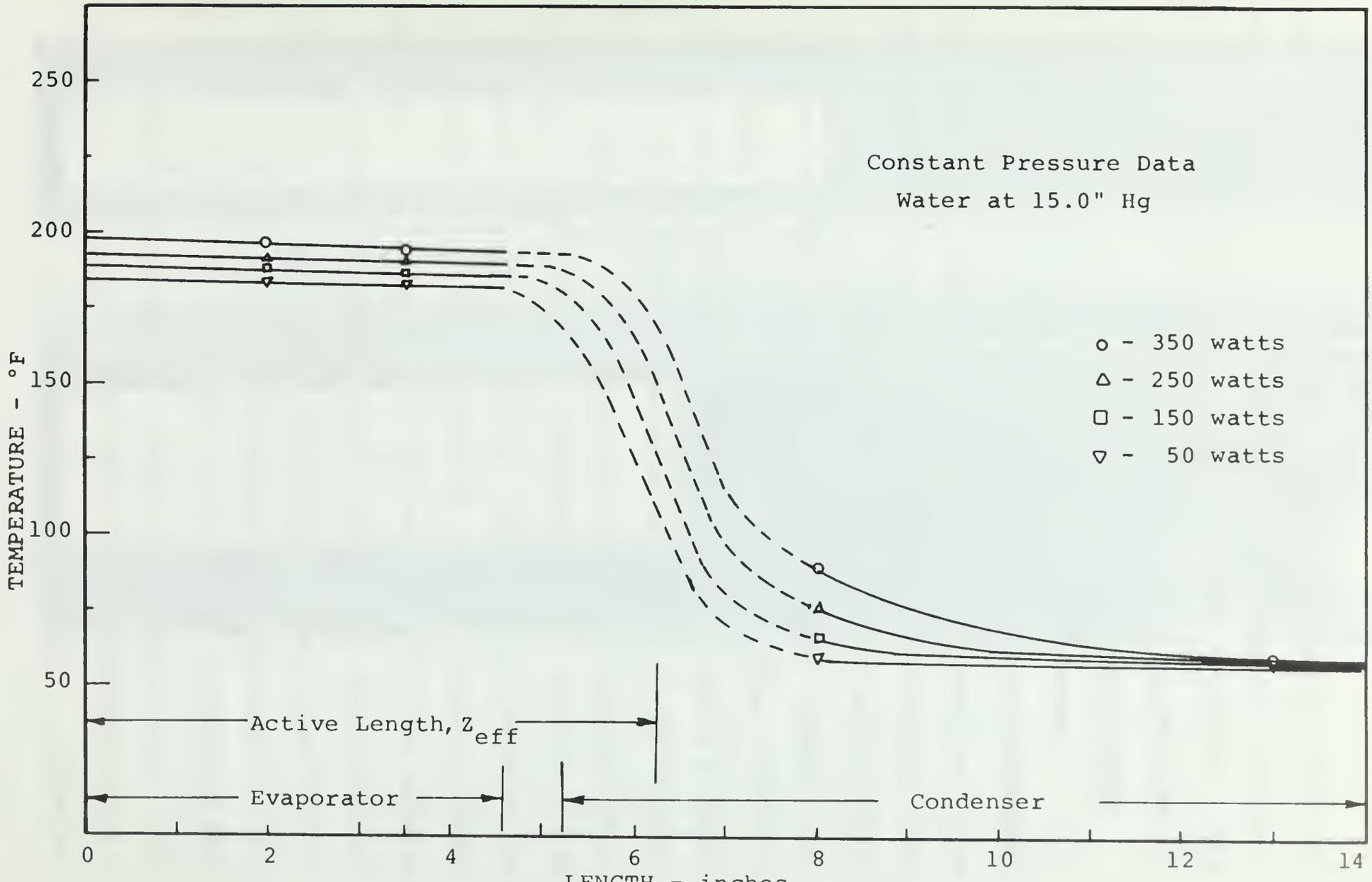

Figure 8. Typical Axial Temperature Profile

dryout the pressure no longer increased since there was no longer an increase in the amount of vapor being added. A type of boiling, described in a later section, also accompanied dryout

Temperature Profile

Theoretically the heat pipe has nearly isothermal temperature profiles in the vapor and also along the pipe wall, not considering the radial temperature gradients of heat entering and leaving the pipe. This was not observed with the pipe under study. A. Carnesale et al. [14], R. T. Burges [15], and others have also observed this non-isothermal performance in low temperature heat pipes. Figure 8 shows typical temperature profiles for different heat fluxes at a constant pressure. Profiles for other operating conditions were quite similar. The exact shape of the profile in the transition region between evaporator and condenser is not known since there were no thermocouples in this region. Therefore this portion of Figure 8 is shown with broken lines and is a profile that may occur. The reason for this rather abrupt temperature change is not entirely known, although the overdesign of the condenser, the presence of noncondensable gas, and high liquid flow resistance all would tend to cause the pipe to operate with a shorter effective length. A moveable thermocouple in both the vapor and the pipe wall, capable of traversing the length of the pipe would be better for determining

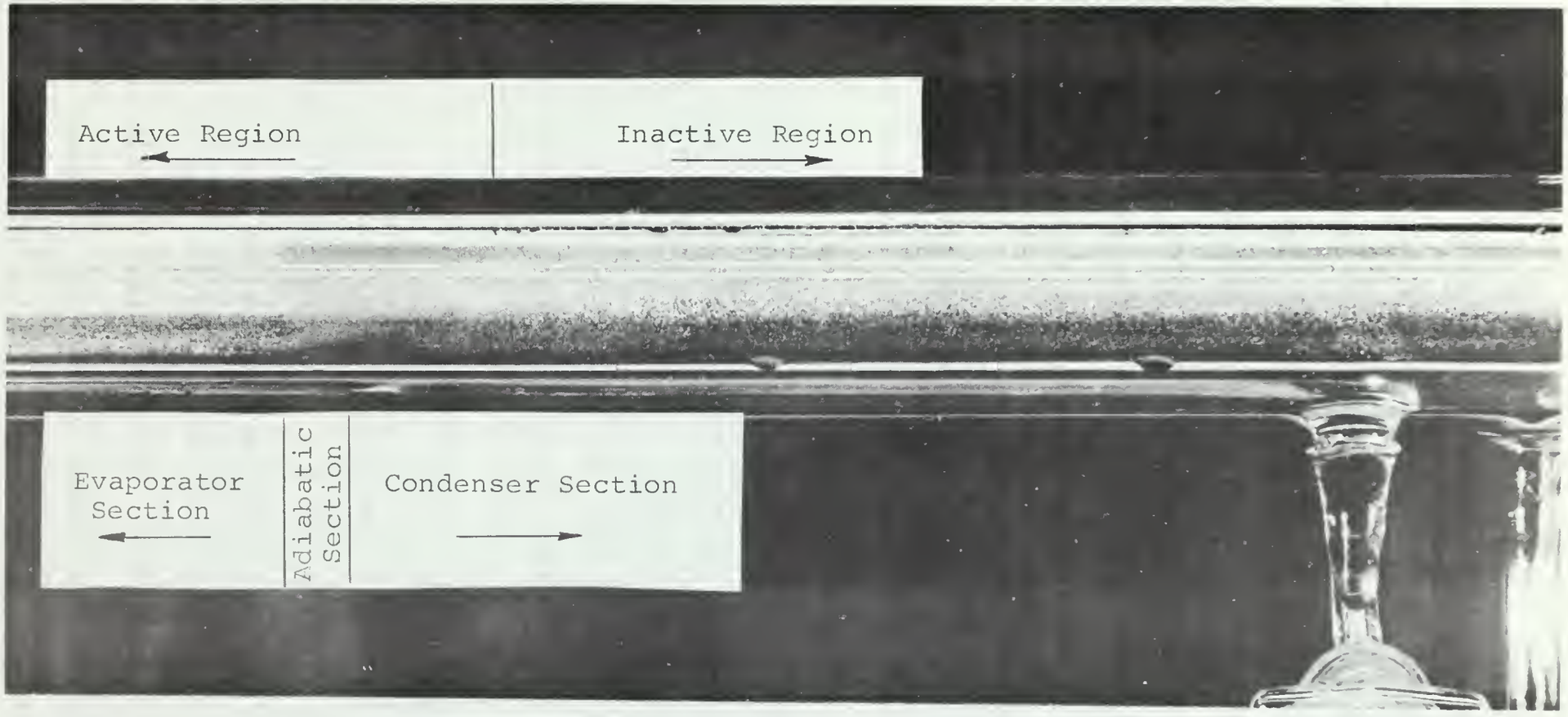

Figure 9. Photograph of Transition Section

the temperature profile. With a completely observed profile this temperature step may be better explained.

Figure 9 is a photograph showing the transition region of the pipe using water, with 150 watts input and 15.0" Hg vacuum. In the evaporator section no liquid is observed in the top layer which was always the case, except at very low heat fluxes. In the condenser section to the extreme right, condensate is noted on the outer layer of wick but no condensing activity is seen. Condensing activity is evident in the condenser end toward the evaporator. The liquid depth in the wick is seen to decrease from this active condensing section across the adiabatic section to the evaporator. These observations suggest that only part of the condenser was in use. The condenser coolant temperature rise was less than one degree Fahrenheit so the condenser surface temperature was nearly isothermal and would have little influence on the above observation.

Surface Orientation

For cylindrical heat pipes in a horizontal position the evaporating surface has all orientations through 180° from the wick above the pipe surface to the wick below the pipe surface. This pipe had thermocouples on both the top and bottom surfaces in the evaporator section making it possible to observe the effect of the two extremes in surface orientation. Kunz, et al. [11] report differences in heat transfer rate with inclination on mesh-covered flat

plates. In this study, on some runs a bottom thermocouple could read slightly higher than a top thermocouple or vice versa on other runs. If a certain location became slightly hotter it usually remained so through the run. Therefore, there was no fixed pattern to the small deviations of some thermocouples from the average evaporator temperature so surface orientation had no effect.

OBSERVATION OF BOILING

Two general types of boiling were observed with the present apparatus, neither of which, in itself, caused any effect on the overall pipe operation.

Incidental Boiling

During normal operation of the pipe a type of boiling was observed in the evaporator wick. This boiling occurred with water at heat fluxes above 10.0 watts per square inch and at pressures of 15.0" Hg and higher. Also it was more prevalent in the earlier hours of pipe operation when the wick still appeared clean and was well wet. This boiling generally went through the following stages with increasing heat flux. Starting at 10.0 watts per square inch bubbles evolved gently through the wick surface in certain spots and in an intermittent manner. With increasing heat flux the bubbling became more rapid. At about 20.0 watts per square inch the bubbles were smaller and activity was observed in lower layers of the wick. This activity appeared as flashes or abrupt

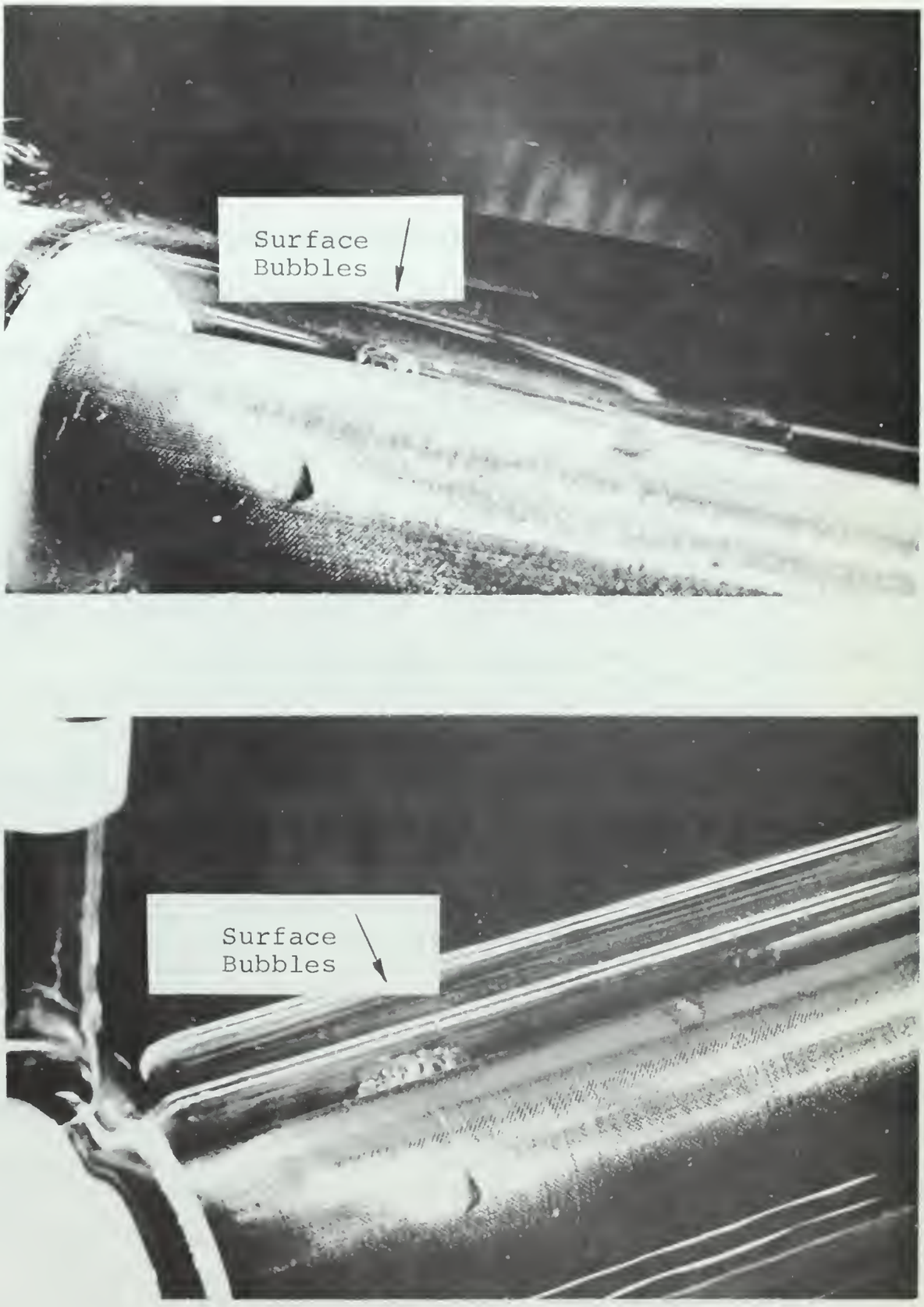

Figure 10. Photographs of Incidental Boiling

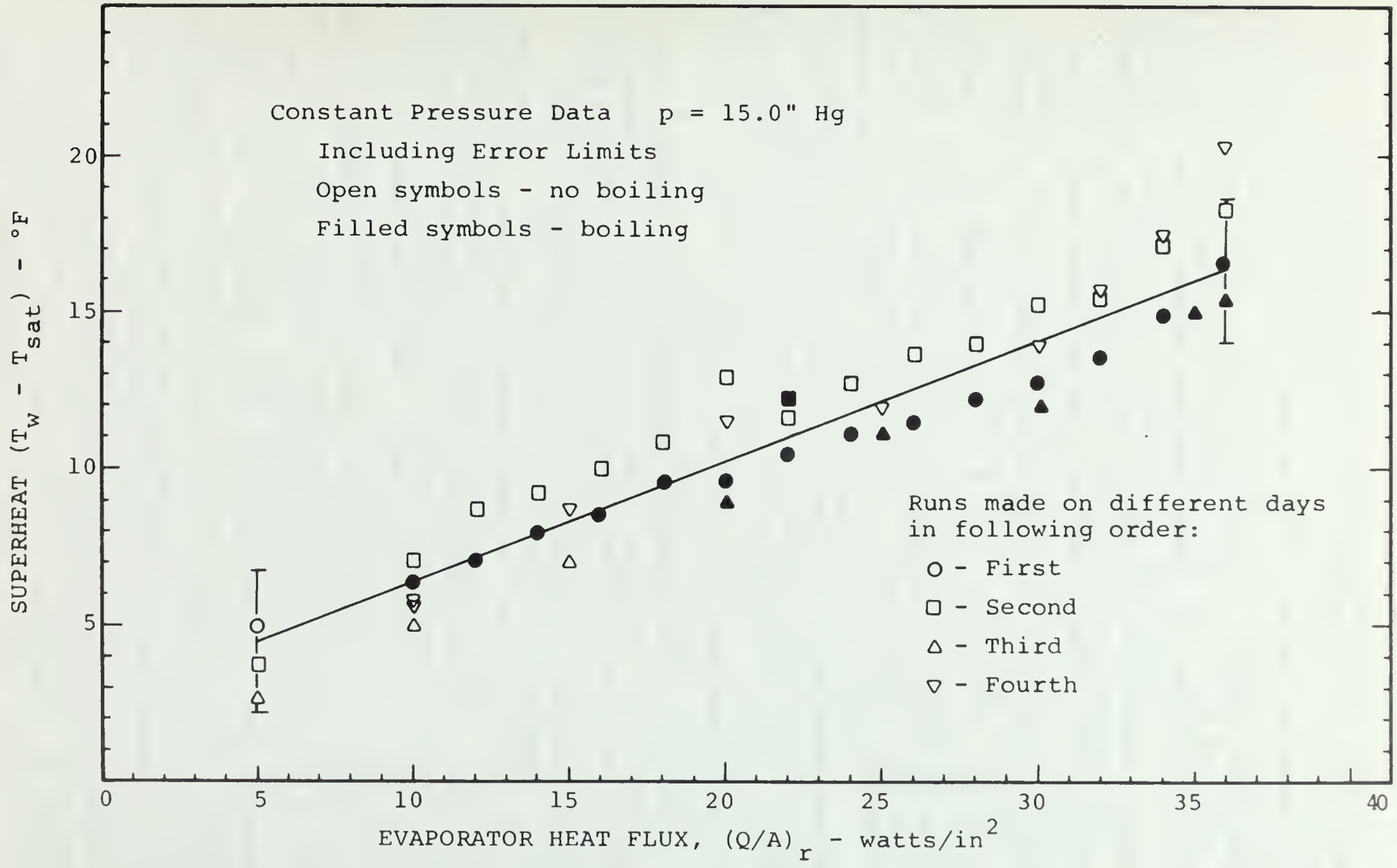

Figure 11. Observed Superheat vs. Radial Heat Flux

waves and will be referred to as sub-layer boiling. At 30.0 watts per square inch on one of the 15.0" Hg runs an occasional audible knocking was noted, like the sound of bubbles forming. As heat flux was increased the surface bubbles became less apparent, sub-layer boiling increased and the knock became less audible and more rapid. Upon reaching dryout at 36.0 watts per square inch the knock was barely detectable with a stethescope and quite rapid. Figure 10 shows photographs of these bubbles at 15.0 watts per square inch and 15.0" Hg vacuum. These are the larger bubbles associated with gentle boiling at the lower heat fluxes. Good photographs were not obtained of the smaller, more rapid bubbles at higher heat fluxes.

Figure 11 shows observed superheat as a function of radial heat flux for four runs at 15.0" Hg. Boiling was observed on two of these runs and is indicated by the filled symbols while the open symbols indicate no boiling. These runs were each done on different days and the boiling was on the first and third runs. Individual data points fall within the expected error limits of the average curve using a 0.95 probability criterion. Points with boiling generally tend to have slightly less superheat than those without boiling, however this could be due to the expected error in measuring and controlling pressure. A discussion of expected errors is given with the error analysis in Appendix B. Therefore, within the limits of expected

error, this type of boiling caused no noticeable effect on the overall operation of the pipe and was thus termed incidental boiling. Boiling could not always be observed when the pipe was brought back to the pressure and temperature conditions that caused it previously.

As more operating time accumulated on the pipe the incidental boiling diminished and finally did not appear at all. Not until the wick was again cleaned did any boiling occur. Thus surface contamination appeared to be a factor in this form of boiling. The surface bubbles and sub-layer boiling could not be detected by sound.

In examining the conditions which cause boiling, equation (8) suggests that a critical value of superheat, $(T_w - T_{sat})$, is necessary. Figure 12 shows critical superheat as a function of vapor pressure with equation (8) using a nucleating radius, r_n, equal to the capillary radius, r_c. This should be conservative and predict the minimum superheat to produce nucleate boiling. The open symbols are the maximum superheats obtained with no boiling and filled symbols are superheats at the incipience of boiling. Some boiling data at the high pressures may be slightly higher than that for incipience of boiling because of the manner in which these points were reached. Values of T_{sat} are those corresponding to the vapor pressure. Since the observed superheats are greater than the theoretical curve, $r_n = r_c = 0.00275"$ must indeed be conservative. Choosing an $r_n = 0.0005"$ causes equation (8)

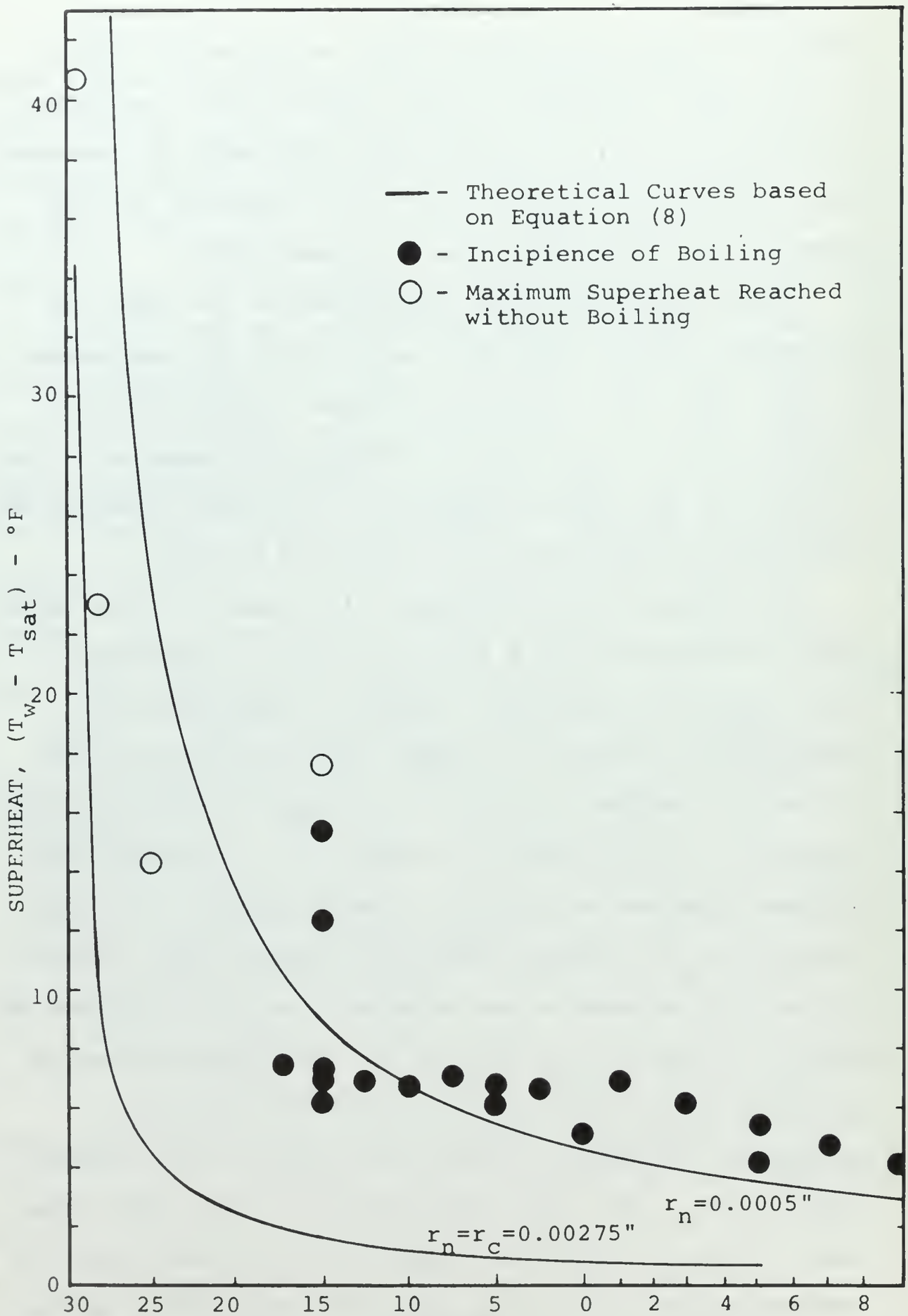

Figure 12. Superheat for Incipient Boiling

to pass reasonably well through these points. Expected error limits are not included since r_n is only an estimate to give the order of magnitude. This idea suggests that the nucleating sites are about one-fifth the size of r_c based on mesh size. Thus for the 100 mesh wick, boiling is dependent on the pipe or wick surface condition and independent of the wick geometry itself.

Dryout Boiling

A second basic type of boiling was that which accompanied dryout caused by the capillary limit. This boiling was caused by liquid covering a spot on the pipe surface which had previously become dry. The result was a rapid boiling with sub-layer flashing and sometimes spitting or expelling droplets out into the vapor space. This boiling appeared to be a result of and not a cause of dryout and could be caused by inclining the pipe so that liquid covered the dried surface.

EFFECT OF PRESSURE

Constant Pressure Data

Since the apparatus was equipped with a means of controlling pressure the majority of the observations were made with a fixed pressure for each run. Runs were made at six different pressures from 29.5" Hg vacuum to 5.0 psig with water as the working fluid. These results are shown in Figure 13 and within the range of normal operation of the pipe the evaporator temperature increases nearly

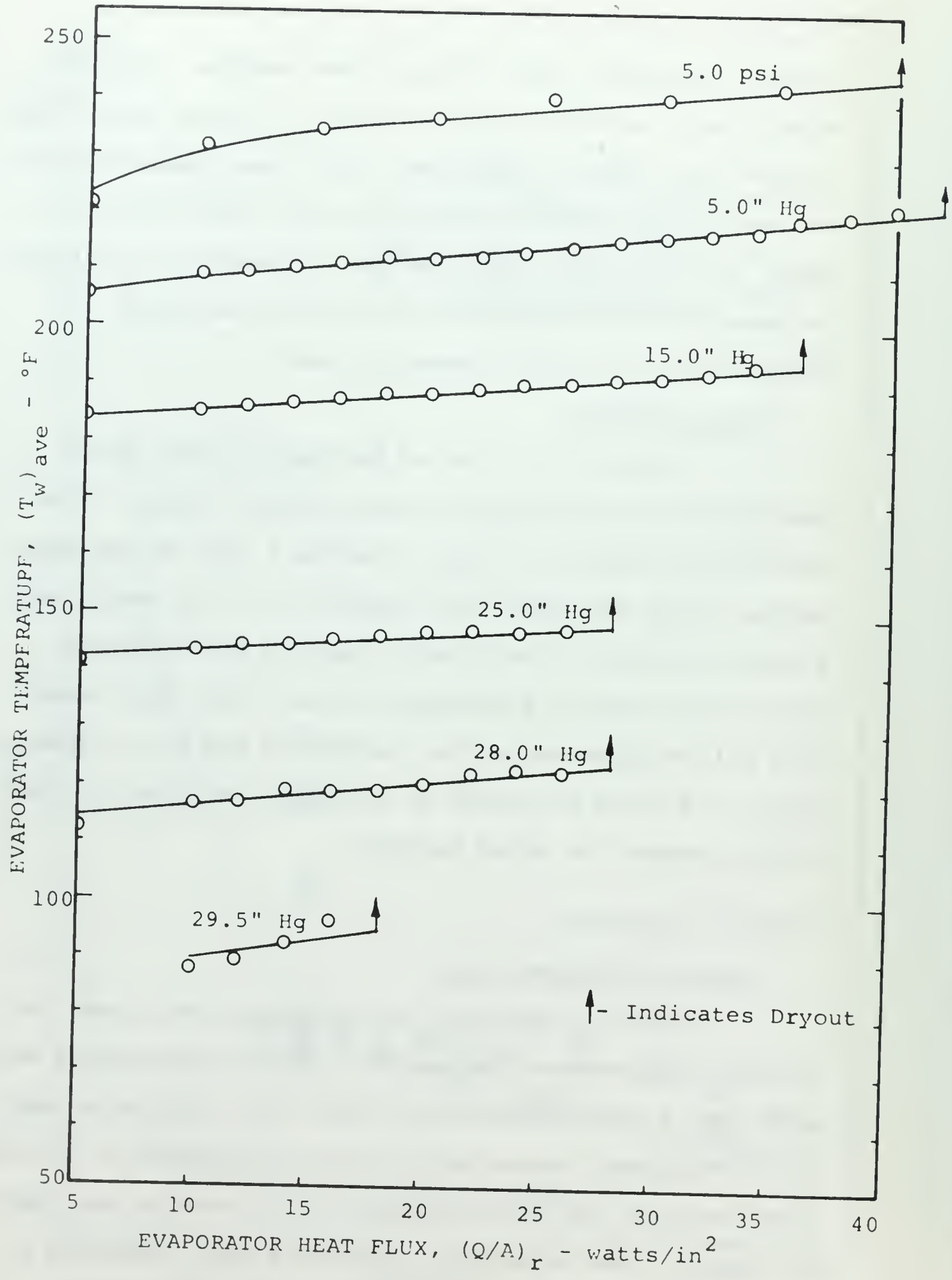

Figure 13. Temperature vs. Heat Flux for Water

linearly with increasing heat flux. Increasing pressure increases the overall operating temperature of the evaporator but has little effect on the rate of temperature change with heat flux. The dryout points are indicated with arrows in Figure 13 and the maximum heat flux generally increases with increase in pressure.

Effective Wick Conductivity and Thickness

It is possible to calculate an approximate effective conductivity of the wick-liquid combination using equation (4). The conductivities of both the liquid and wick material increase slightly with temperature, but within the small range of temperatures in each run these properties can be considered constant.

The liquid level in the evaporator will decrease with an increase in heat flux. As the liquid recedes into the lower layers of the wick the upper layers are exposed to vapor. If these upper layers are then assumed to be at the vapor temperature the effective wick thickness has been reduced. Equation (6) can be written in the form

$$\frac{R_v'}{R_w} = \exp\left[\frac{K_{eff} A (T_w - T_{sat})}{R_w Q}\right] \qquad (12)$$

where R_v' is an effective wick radius.
With observed values of Q, $(T_w - T_{sat})$, and k_{eff} from equation (4) the effective R_v' can be determined. Effective wick thickness is then

$$d = R_v' - R_w \tag{13}$$

When the thermal conductivity of stainless steel is used for k_w in equation (4), the effective wick thickness calculated from equations (12) and (13) is larger than the actual wick thickness. This indicates k_w must be lower as discussed in Section II. Choosing $k_w = 0.25\ k_{ss}$ produces the effective wick thickness curve in Figure 14. Visual observation tends to verify this. With a very low heat flux liquid can be seen near the wick surface in the evaporator and at higher heat fluxes the sub-layer flash appears to be about one or two layers from the wick surface. Effective thickness is seen to decrease exponentially with increasing heat flux. Other pressures also give this general magnitude for d. As this effective wick thickness becomes smaller the flow area for returning condensate is reduced which contributes to the dryout limitation. When dryout occurs this wetted wick thickness becomes less than that necessary to support steady operation.

If the data with incidental boiling in Figure 11 did in fact have a slightly lower superheat than without boiling, then the effective wick thickness was slightly lower with that type of boiling. More observations of the incidental boiling would be needed to verify this.

Maximum Heat Transfer

The maximum heat transfer at each pressure was determined as the point where dryout was impending. This

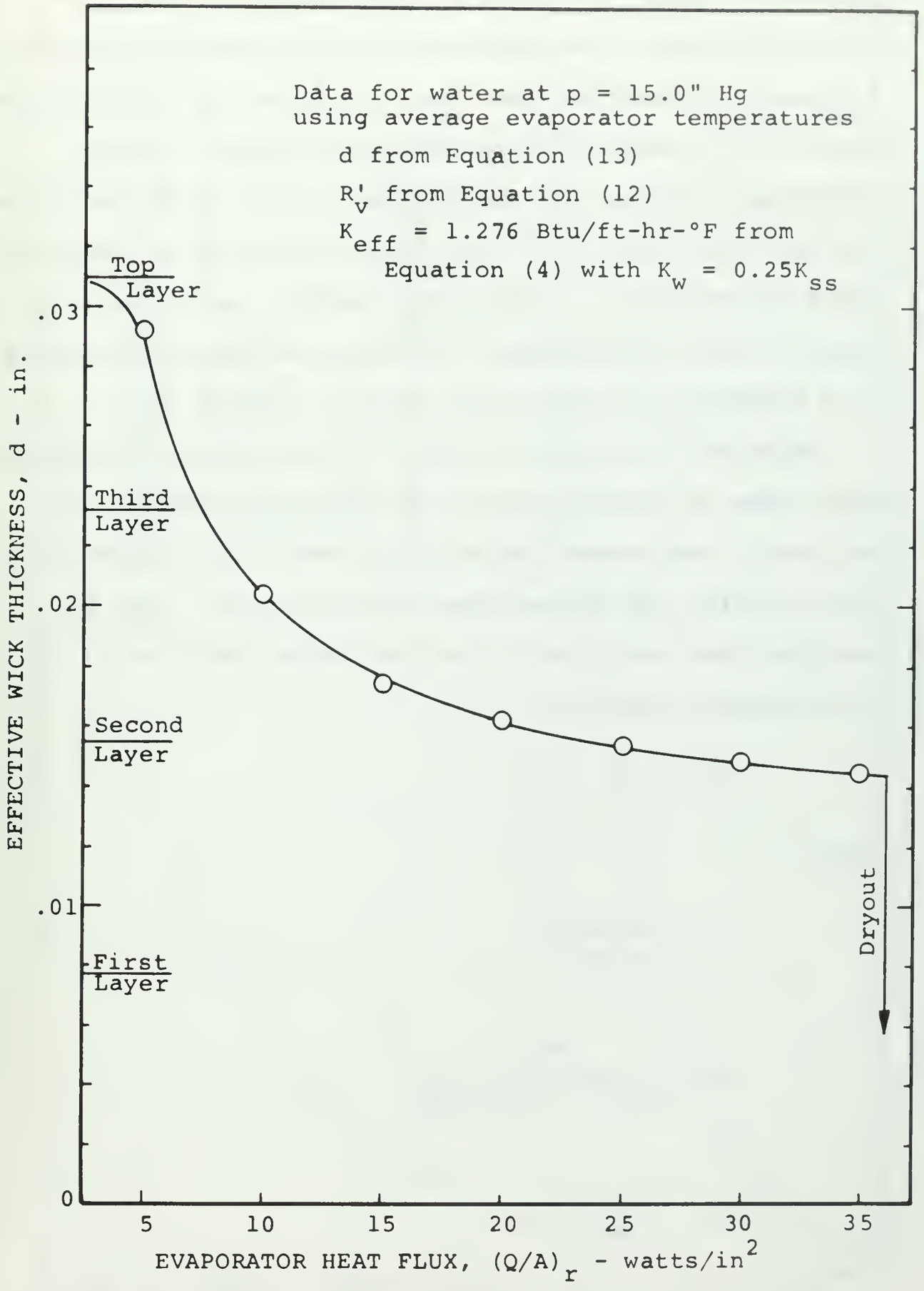

Figure 14. Effective Wick Thickness in Evaporator

point was found to be reproducible if the power input was increased gradually. Most runs were made with power increments of 20.0 watts and data was taken after a steady operating condition was established. Under such conditions the four runs with 15.0" Hg vacuum were found to reach 360 watts before dryout. This point was then used as a reference in later calculations. Observed maximum power points as a function of pressure are shown in Figure 15.

Solution of equation (1) for the case where the pressure drop terms on the right equal the capillary pumping term and taking the contact angle to approach zero in the evaporator yields the maximum heat transfer rate. This was done for this heat pipe in the horizontal position giving the following equation:

$$AQ^2 + BQ - C = 0 \tag{14}$$

where

$$A = \frac{(1 - 4/\pi^2)}{8\rho_v R_v^4 L^2}$$

$$B = \frac{b\mu Z}{2\pi(R_v^2 - R_w^2)\rho_\ell \varepsilon r_c^2 L}$$

$$C = \frac{2\gamma \cos\theta}{r_c}$$

Equation (14) is a quadratic form, however, as seen in the sample calculations in Appendix A, the term due to

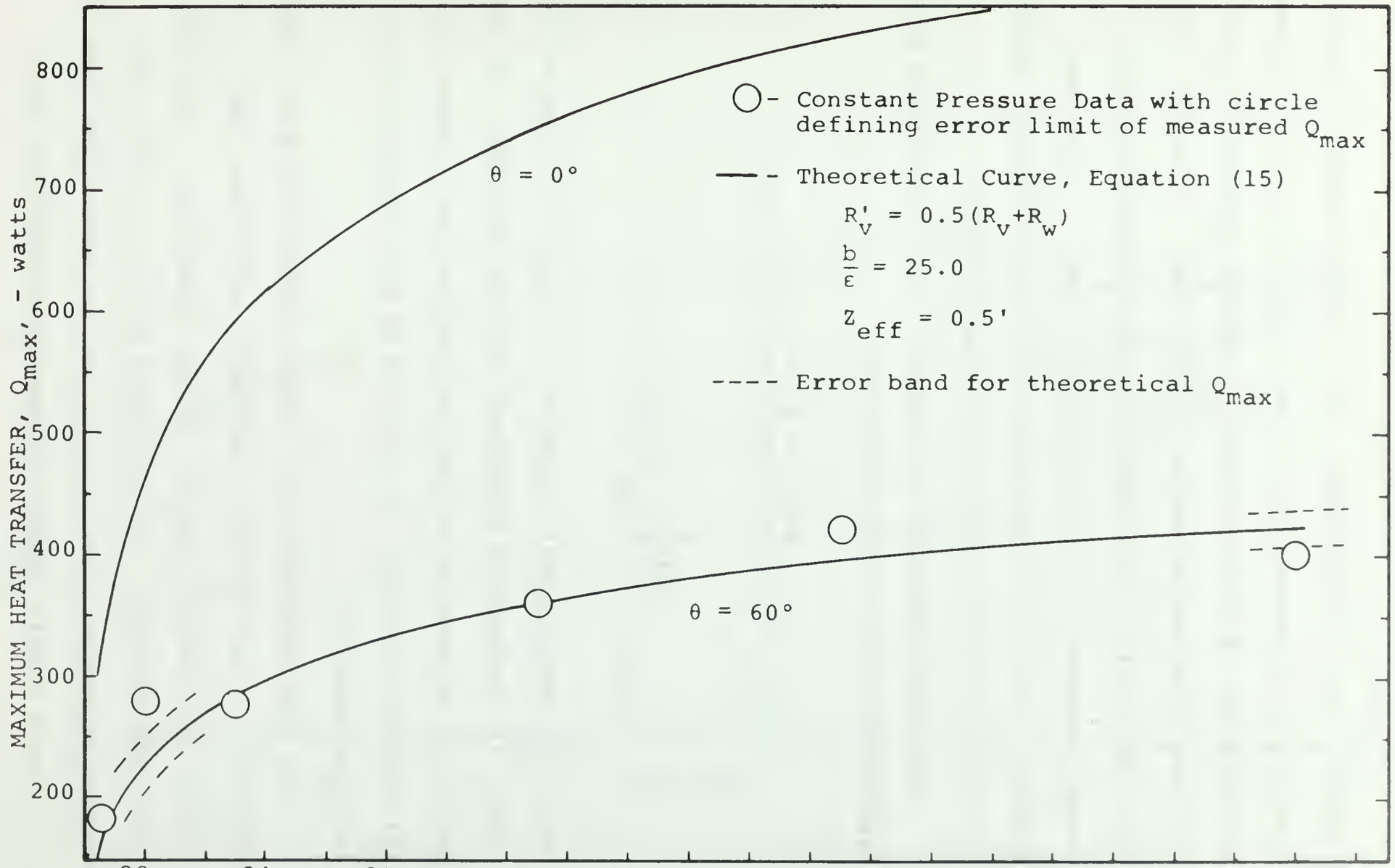

Figure 15. Maximum Heat Transfer vs. Pressure for Water

pressure drop in the vapor, AQ^2, is much smaller than the term due to pressure drop in the liquid, BQ. Such a form is difficult to solve directly, however disregarding the AQ^2 term gives solutions for Q which are in error by only 0.27% to 0.06%. The relatively large magnitude of the liquid pressure drop term indicates that the pipe was limited by the high resistance to flow and capillary pumping ability of the wick and not by other factors.

With simplification of equation (14) the maximum heat transfer is given by equation (15)

$$Q_{max} = \frac{C}{B} = \frac{4\pi(R_v^2 - R_w^2)\varepsilon r_c}{bZ} \cdot \frac{\rho_\ell L\gamma}{\mu} \cdot \cos\theta$$

$$Q_{max} = \frac{4\pi(R_v^2 - R_w^2)\varepsilon r_c}{bZ} \cdot N \cdot \cos\theta \qquad (15)$$

Therefore maximum heat transfer rate is a function of three terms, (1) parameters dependent on pipe geometry, (2) working fluid parameters defined earlier as the N number, and (3) the wetting angle, a function of both working fluid and pipe material.

The pipe parameters are fixed, however the pipe could operate so that effective values of length and vapor space radius are smaller than the actual dimensions. The effective wick thickness was discussed earlier. Since this wetted thickness determines the axial liquid flow area, it is more nearly correct to use R_v' in equation (15).

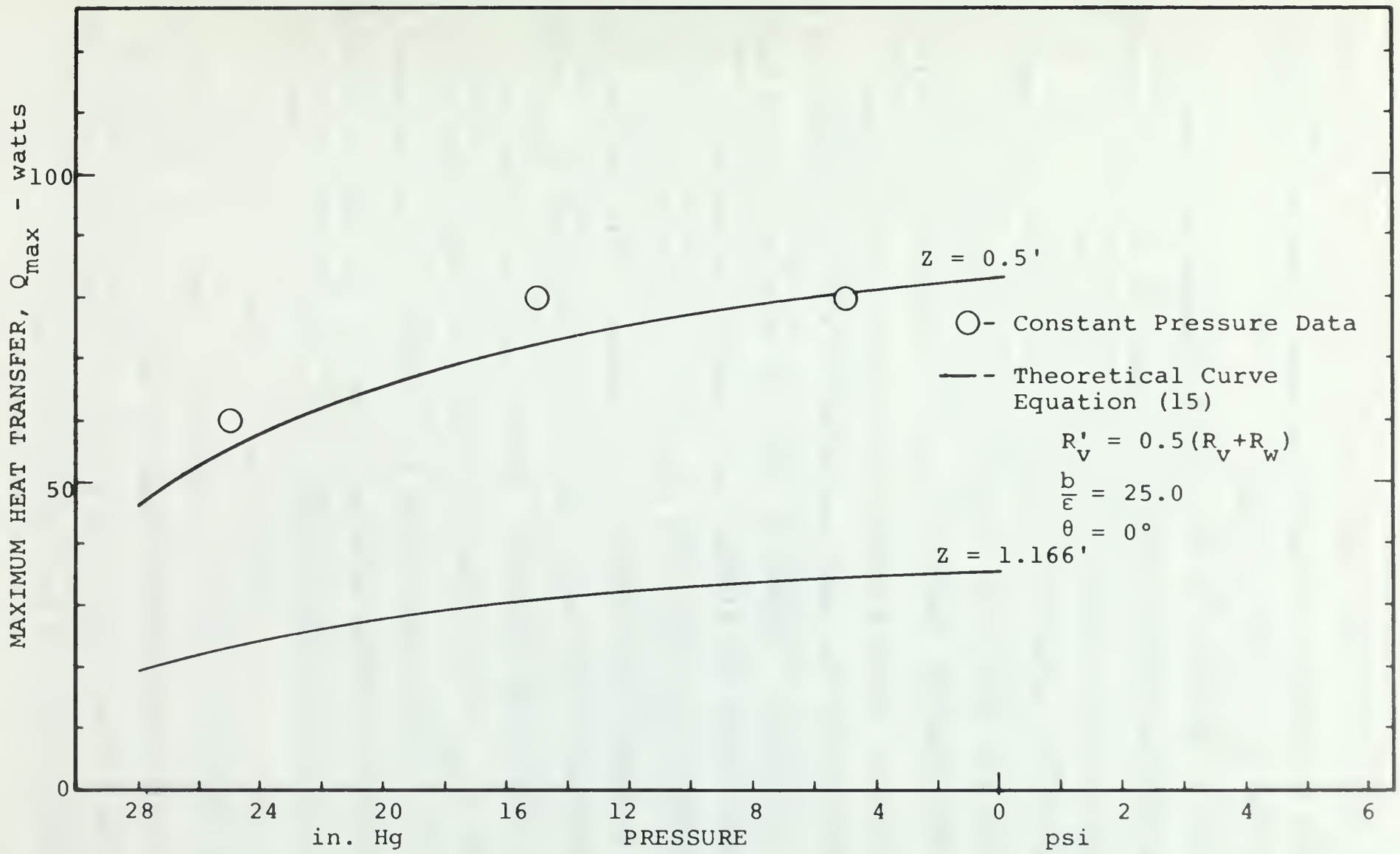

Figure 16. Maximum Heat Transfer vs. Pressure for Ethyl Alcohol

This effective vapor space radius was noted to have little change at the higher heat fluxes near dryout so a constant value of $R_v' = 0.390"$ was used.

The b parameter in the liquid pressure drop term is a dimensionless constant depending upon the detailed geometry of the wick and is generally in the range of 10 - 20. A value of $\frac{b}{\varepsilon} = 25$ for the 100 mesh wick will be used based on data for other mesh screens reported by Ernst [11].

The effective length, Z_{eff}, was determined in the following way. Since alcohol was found to have very good wettability on the stainless steel, $\theta = 0°$ was assumed in the evaporator. Figure 16 shows the observed maximum heat transfer rates for alcohol as a function of pressure. A theoretical Q_{max} curve was obtained by using equation (15) with N values as a function of pressure. This theoretical curve based on the actual pipe length predicted Q_{max} values lower than those observed. However using an effective length, $Z_{eff} = 0.5'$ puts the theoretical curve reasonably close to the observed values for alcohol. Since the axial temperature profiles were approximately the same for alcohol and water the effective length was considered the same for each liquid. A Z_{eff} of 0.5' is in agreement with the active section of pipe as observed in Figure 9. The effective length being shorter than the actual length explains the step in the temperature profile although the conditions determining Z_{eff} are not completely known.

For water a theoretical Q_{max} vs. pressure curve using Z_{eff} and $\theta = 0°$ is shown in Figure 15. Since this curve predicts values greater than those observed the wetting angle may be different. Water was observed to have poor wettability on the wick with drops sometimes beading up rather than being absorbed into the wick. If θ is adjusted so that the theoretical curve predicts Q_{max} = 360 watts at 15.0" Hg then this curve fits all the observed data within the expected error limits. The wetting angle thus determined is 60°.

Pressure Control System

With the inclusion of the pressure adjuster, the heat pipe operating point could easily be controlled. Figure 17 shows the effect on evaporator wall temperature of varying the pressure with the pressure adjuster. The curve is seen to nearly parallel the saturation temperature curve, indicating a relatively constant amount of superheat over the pressure range considered. This data was found to be quite reproducible, i.e. with a fixed amount of air in the system a given volume setting on the adjuster produced the same pressure and temperature regardless of the previous operating point.

The system was also found to respond reasonably fast to change from one point to another on this curve. Figure 18 shows this response in changing pressure from 20.0" Hg vacuum to 11.0 psi and back to 20.0" Hg vacuum. This is

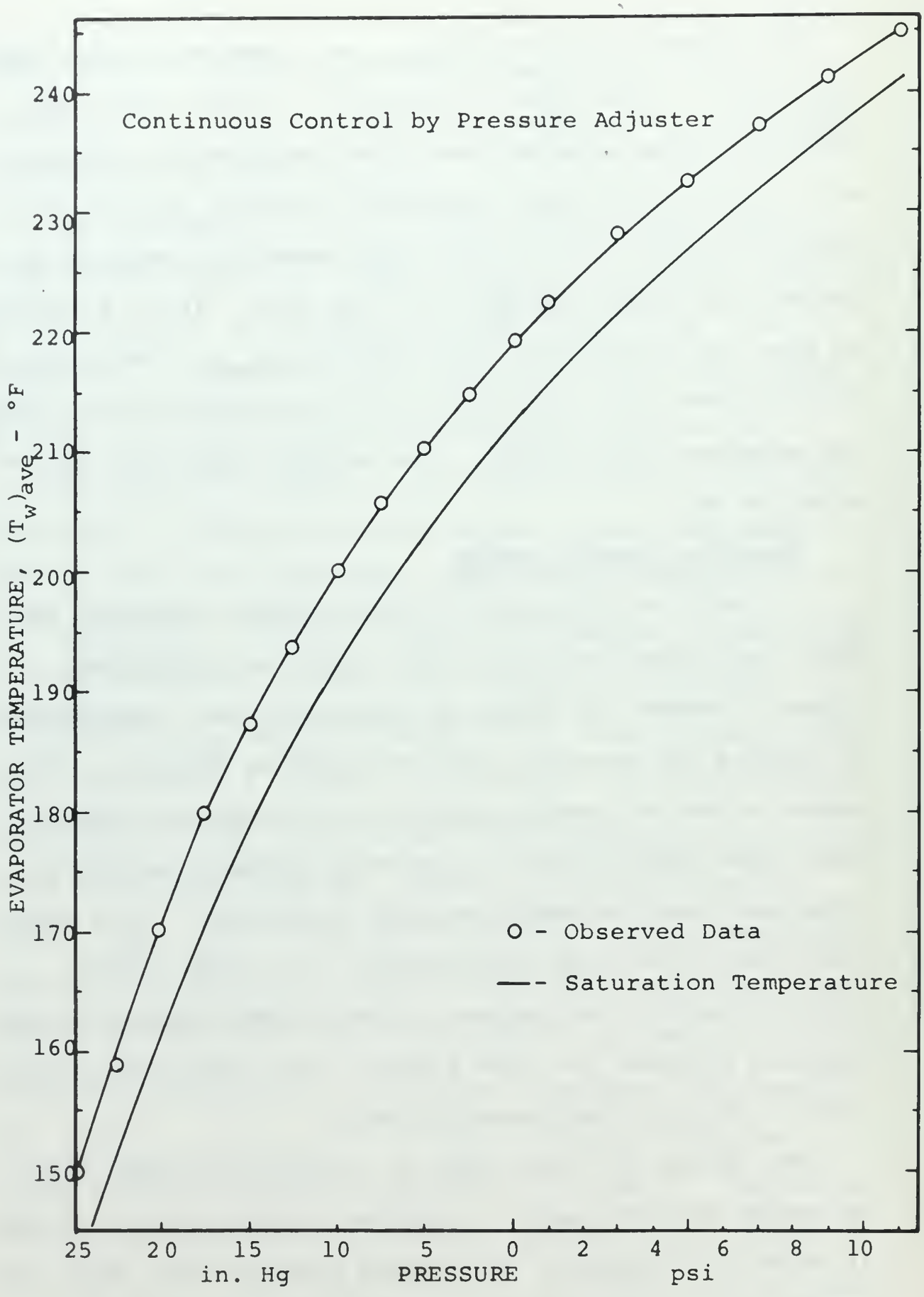

Figure 17. Effect of Pressure on Evaporator Temperature

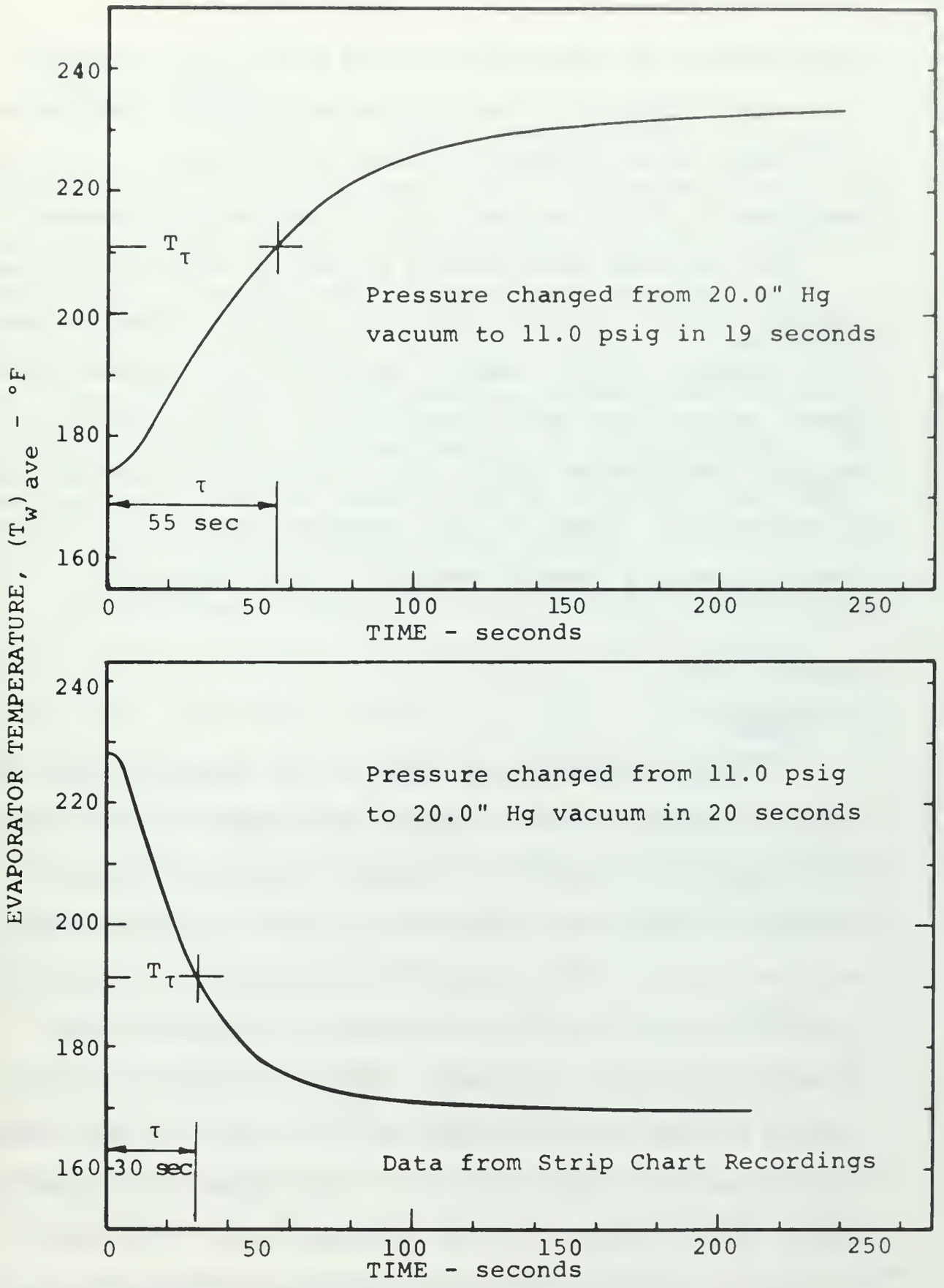

Figure 18. Time Response of Heat Pipe to Pressure Change

approximately an exponential curve with a time response of τ = 55 seconds for the increasing pressure case where the actual volume change was made in 19 seconds. The time response, τ, is 30 seconds for the decreasing pressure.

Thus the heat pipe becomes an easily controllable heat transfer device with the addition of such a pressure control system. In this case of constant heat transfer the source temperature can be controlled. In the case of a constant temperature source the rate of heat transfer will be controlled. Study of this constant temperature source case with such a control system would be desirable.

WORKING FLUID

Water

Distilled water was used as the working liquid for most of the runs and the overall performance in the pipe has been presented in earlier sections. Generally, water appeared to have poor wettability on the stainless steel. This was noted in the behavior of the water on initially filling the wick and also in behavior of droplets when splashed on the wick surface. Droplets tended to bead up showing a large contact angle and often ran off the surface rather than down into the wick. Also condensate tended to remain on the surface in the condenser end. This poor wettability was particularly noted after the pipe had set a few days and when the water was used in the pipe following operation with alcohol.

Ethyl Alcohol

For comparison a second working fluid, 190 proof denatured ethyl alcohol, was used. The wettability of the alcohol was much better. Droplets splashed on the wick were immediately absorbed and no condensate was seen on the surface in the condenser. Figure 19 shows the temperature vs. heat flux behavior at constant pressure for the ethyl alcohol. This behavior is similar to that of water. The maximum heat transfer rates shown in Figure 16 are from one-fifth to one-third those with water.

The N parameter defined in equation (2) suggests that water should be much more effective in heat transfer capability than ethyl alcohol. At 15.0" Hg vacuum, for example, $N_{alcohol} = 15.5$ and $N_{water} = 309.5$, or water should be 20 times as effective. At this pressure the experimental data indicates that water was only 4.5 times as effective, the difference being due mainly to the poor wettability of water on stainless steel.

No wick surface bubbling was observed with alcohol, but the sub-layer flashing was noted. Although this sub-layer activity was readily observable it did not have sufficient contrast to show on the photographs. Also the alcohol tended to have more boiling connected with dryout. This was probably because the good wettability of the alcohol caused small amounts of condensate to return to the already dry spots of the evaporator.

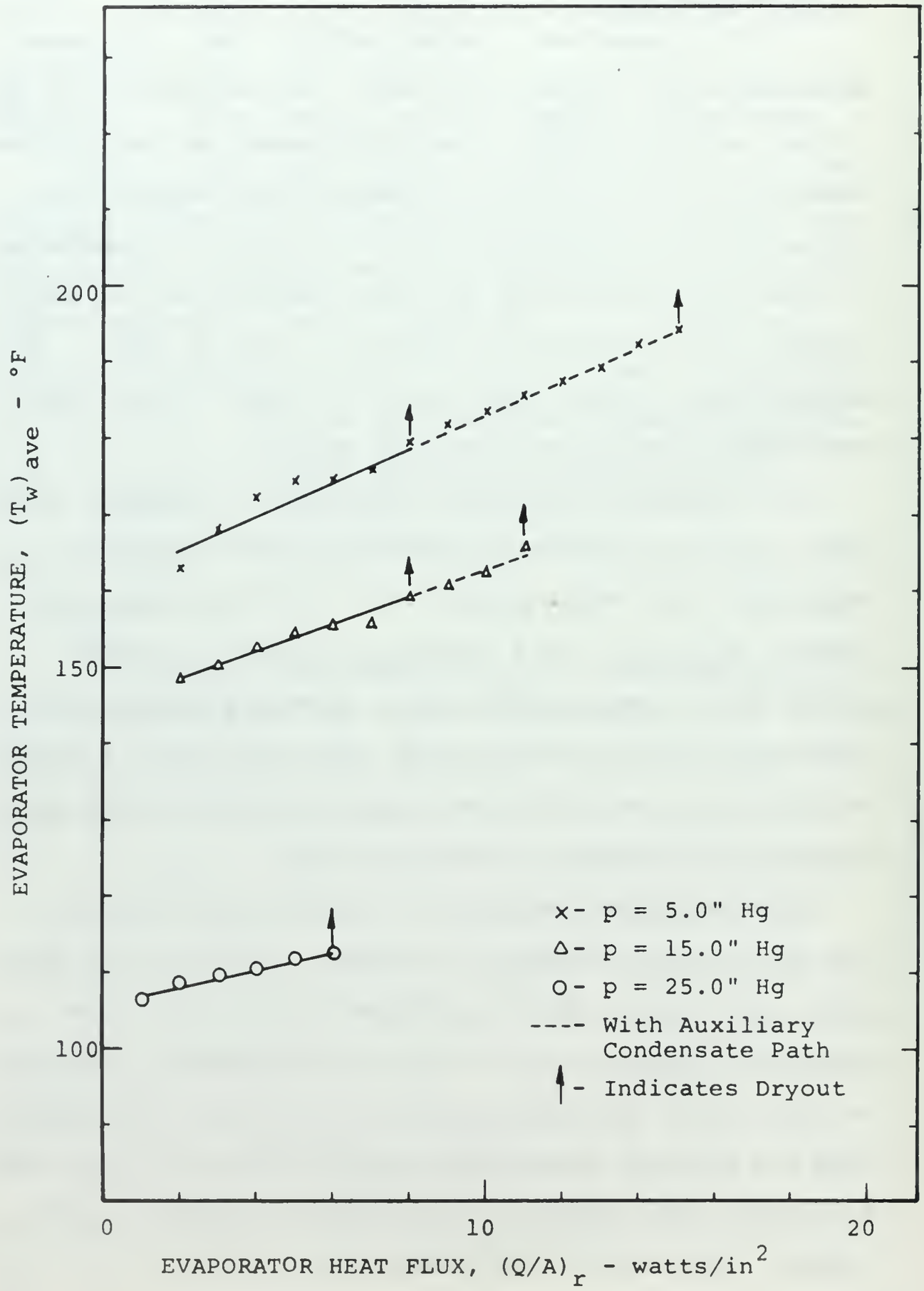

Figure 19. Temperature vs. Heat Flux for Ethyl Alcohol

AUXILIARY CONDENSATE PATH

The auxiliary condensate path provided by the small fiberglas cloth wick in the evaporator end of the pipe was described in Section III. The maximum heat fluxes discussed thus far were obtained with the condensate returning through the main wick only. When the excess condensate pool in the bottom of the vapor chamber was allowed to touch the fiberglas wick, condensate was supplied by this auxiliary path to the far end of the evaporator. With this additional condensate the pipe was able to operate to higher heat fluxes as shown with the dashed lines in Figure 18. In one case it almost doubled the maximum heat flux attained. This effect was also observed with water but the increase in maximum heat flux was not as great.

This again indicates that the maximum heat flux was limited by high flow resistance in the wick and capillary pumping ability. Since this auxiliary condensate path serves the same function as axial grooves and arteries, it can be inferred that these improved wick geometries will perform much better than the all-mesh wick.

SMALL ANGLE INCLINATION

Most of the runs in this study were made with the pipe in a horizontal position to minimize the effect of gravity while other variables were being considered. However for a comparison of how this pipe would work at small angles

of inclination some observations were made. Runs were made with water, at an angle of inclination $\phi = +3°$, and $p = 15.0"$ Hg and $25.0"$ Hg. Inclination angle was measured counterclockwise from the horizontal with the evaporator end up. This small angle caused both an increase in the rate of temperature increase with increasing heat flux and a lower maximum heat flux as seen in Figure 20. With alcohol as the working fluid, $p = 25.0"$ Hg, and $\phi = -3°$ the temperature rise with increasing heat fluxes was about the same as $\phi = 0°$ but the maximum heat flux was considerably higher.

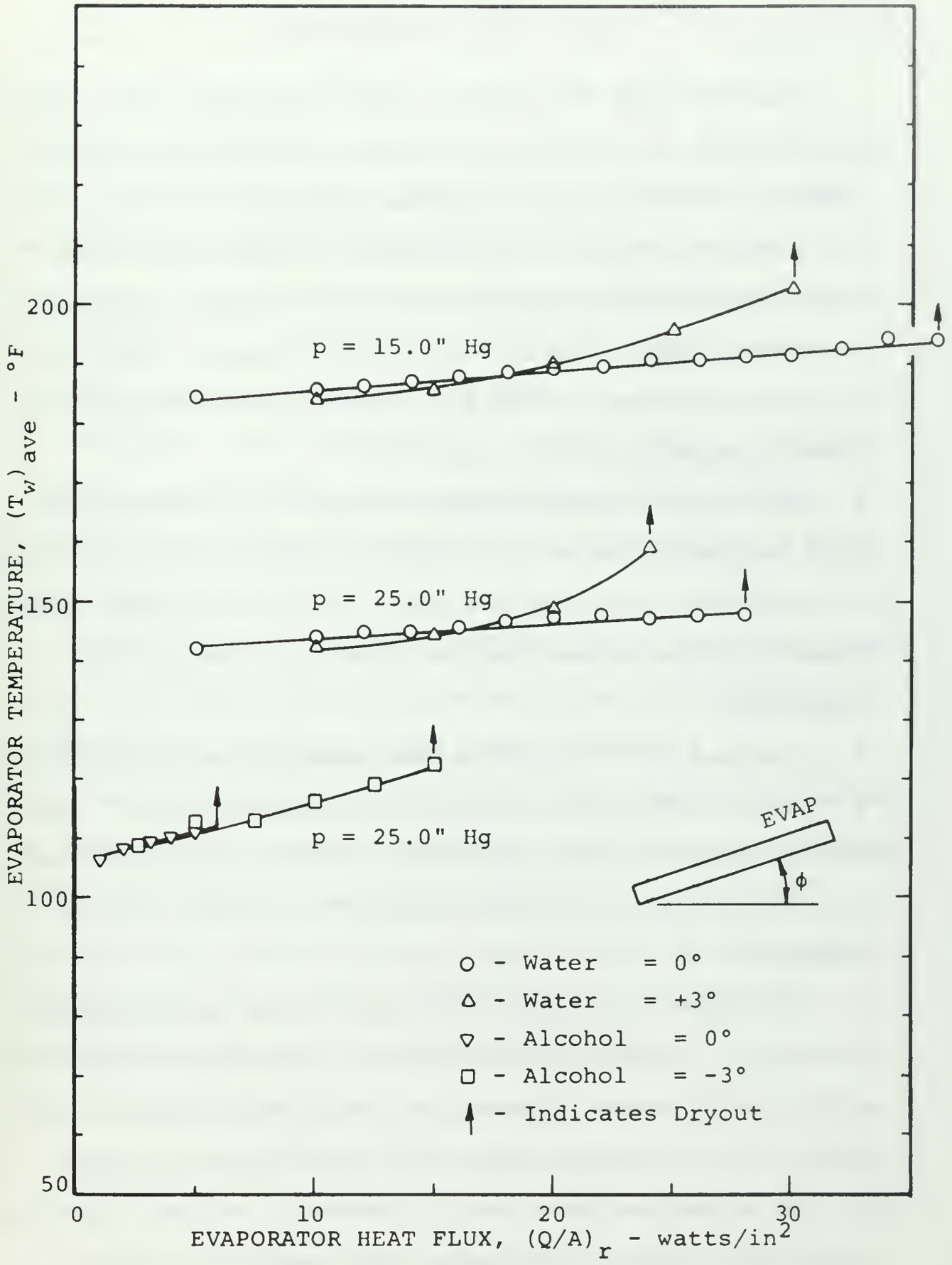

Figure 20. Effect of Small Angle Inclination

VI. CONCLUSIONS

1. The heat pipe with four layers of 100 mesh wire cloth wick used in this study was limited by capillary pumping ability and high liquid flow resistance in the wick.
2. A type of boiling was observed at higher pressures which appeared to have no effect on the overall operation of the heat pipe. This gentle form of boiling would not have been detected if the pipe had not been designed for visual inspection of the wick.
3. Boiling was observed under conditions which suggest that the nucleating active sites had radii about one-fifth the capillary radius of the wick. Boiling was more likely caused by pipe or wick surface condition than by wick geometry.
4. A second form of boiling was caused by wick dryout as a result of exceeding the capillary pumping limit. This was a vigorous boiling as liquid covered a hot, previously dry surface and, in itself, produced no effect on pipe operation.
5. The effective wick thickness or wetted depth appeared to steadily decrease with increased radial heat flux. This effective thickness appeared to reach about one-half the actual wick thickness before the pipe failed by dryout.
6. The effective pipe length appeared to adjust itself to obtain the amount of condenser area needed when non-condensable gas was present in the vapor space.

7. There can be relatively large uncertainties in various parameters of the pressure balance equation, including those often considered constant, such as the wetting angle θ, the $\frac{b}{\varepsilon}$ characteristic, effective length Z_{eff}, and effective vapor space radius, R_v'. The everted heat pipe provided maximum heat transfer rates close to those predicted by the theory for the similar cylindrical pipe using $\frac{b}{\varepsilon} = 25.0$, $R_v' = \frac{R_v+R_w}{2}$, $Z_{eff} = 0.5'$, and $\theta = 0°$ for alcohol and $\theta = 60°$ for water on stainless steel.

8. Stainless steel surfaces can easily become contaminated and can greatly affect the wettability by water, thus hindering the proper operation of a water-stainless steel heat pipe.

9. Ethyl alcohol has better wettability on stainless steel than does water but alcohol is still several times less effective as a working fluid than is water.

10. Heat pipe operating conditions can readily be changed by changing the internal pressure in the pipe. A heat pipe with some form of pressure adjuster can be regulated to transfer heat from a constant power source at a selected temperature, or it can transfer heat from a constant temperature source at a selected heat flux.

VII. RECOMMENDATIONS FOR FURTHER STUDY

1. With the everted heat pipe as designed many variations can be made in wick structure. For further study of nucleate boiling, structures which will not limit operation by capillary pumping or high liquid flow resistance are recommended. Some possibilities are:

    a. Increase the thickness of the 100 mesh wire cloth wick to eight or nine layers which is near the theoretical optimum.

    b. Increase wick thickness to 12 layers of 100 mesh wire cloth.

    c. Add four layers of 400 mesh wire cloth over four layers of 100 mesh wick.

    d. Use four layers of 35 mesh wire cloth.

    e. Use alternate layers of 50 mesh and 200 mesh wire cloth.

    f. Use axial grooves covered with wire cloth.

2. Build a similar apparatus using nickel since nickel normally has better wettability than stainless steel.

3. Try other working fluids such as methyl alcohol and freons.

4. Provide a traversing thermocouple in the pipe wall and in the vapor space such that the axial temperature profiles can be better observed.

5. Provide a relatively simple electronic control circuit for the power input so that the evaporator surface could

be maintained at a constant temperature. Heat pipe performance in conjunction with a constant temperature source could then be studied.

6. Investigate further the characteristics and applicability of the controllable heat pipe.

REFERENCES

1. Eastman, G. Y., "The Heat Pipe," Scientific American, p. 38-46, May 1968.

2. Thompson, D. C., Patent Disclosure No. 48148, 10 February 1960.

3. Grover, G. M., Cotter, T. P., and Erickson, G. F., "Structures of Very High Thermal Conductance," Journal of Applied Physics, v. 35, p. 1990 - 1991, 1964.

4. Air Force Flight Dynamics Laboratory Report AFFDL - TR - 66 - 228, Cryogenic Heat Pipe, by W. L. Haskin, June 1967.

5. Los Alamos Scientific Laboratory LA - 3211, High Thermal Conductance Devices Utilizing the Boiling of Lithium or Silver, by J. E. Deverall and J. E. Kemme, 1965.

6. Lawrence Radiation Laboratory, University of California, Livermore, UCRL - 50453, A Critical Review of Heat Pipe Theory and Applications, by H. Cheung, 15 July 1968.

7. Bähr, A., Burck, E., and Hufschmidt, W., Liquid - Vapour Interaction and Evaporation in Heat Pipes, Second International Conference on Thermionic Electrical Power Generation, May 1968.

8. Los Alamos Scientific Laboratory, University of California, Los Alamos, LA - 3246 - MS, Theory of Heat Pipes, by T. P. Cotter, February 1965.

9. TRW Space Technology Laboratories Report No. 9895 - 6001 - TU - 000, On the Operation of Heat Pipes, by B. D. Marcus, May 1965.

10. Lewis Research Center, NASA CR - 812, Vapor - Chamber Fin Studies, Transport Properties and Boiling Characteristics of Wicks, by H. R. Kunz, L. S. Langston, B. H. Hilton, S. S. Wyde, and G. H. Nashick, June 1967.

11. Ernst, D. M., Evaluation of Theoretical Heat Pipe Performance, paper presented at the 1967 Thermionic Conversion Specialist Conference, Palo Alto, California, October 30 - November 1, 1967.

12. Katzoff, S., Notes on Heat Pipes and Vapor Chambers and Their Application to Thermal Control of Spacecraft, paper presented at AEC/Sandia Heat Pipe Conference, October 1966.

13. Hsu, Y. Y., On the Size Range of Active Nucleation Cavities on a Heating Surface, paper presented at the Winter Annual Meeting of the American Society of Mechanical Engineers, New York, N. Y., November 26 - December 1, 1961.

14. Carnesale, A., Cosgrove, J. H., and Ferrell, J. K., Operating Limits of the Heat Pipe, paper presented at AEC/Sandia Heat Pipe Conference, October 1966.

15. Burges, R. T., Design and Operation of a Heat Pipe, M. S. Thesis, Naval Postgraduate School, Monterey, 1968.

APPENDIX A

SAMPLE CALCULATIONS

1. CONSTANT VALUES

Pipe radius,	$R_w = 0.375"$
Vapor space radius,	$R_v = 0.405"$
Pipe length,	$Z = 1.166'$
Evaporator length	$Z_e = 0.354'$
Thermocouple sheath diameter,	$d_t = 0.031"$
Mesh size	$M = 100$
Mesh wire diameter	$d_w = 2r_w = 0.0045"$
Thermal conductivity stainless steel	$k_{ss} = 10.0 Btu/hr\text{-}ft\text{-}°F$

2. SAMPLE CALCULATIONS
(For water at 15.0" Hg unless otherwise noted)

a. Pipe Surface Temperature

Using the cylindrical conduction equation the measured temperature, T_t, can be extrapolated to the surface

$$T_w = T_t - \frac{Q \ln(\frac{R_w}{R_t})}{2\pi Z_e k_{ss}}$$

Assuming the thermocouple junction is one-half the sheath diameter from the surface, $R_t = R_w - \frac{d_t}{2}$

$$T_w = T_t - \frac{\ln(\frac{0.375}{0.3595})}{2\pi(0.354)(10.0)(3.412)} = T_t - 0.000563Q \quad [°F]$$

where Q is in watts

For Q = 50 watts: $T_w = T_T - 0.028$ [°F]

b. Capillary Radius

From equation (3)

$$r_c = \frac{1}{2M} - r_w$$

$$r_c = \frac{1}{2(100)} - \frac{0.0045}{2} = 0.00275" = 0.000229'$$

c. Void Fraction

Void fraction is the void space divided by the volume of the entire wick. The void space is the volume of the wick, V_t, less the volume of the wire in that space, V_w.

On one square inch of surface with four layers of wire cloth:

$$V_t = (R_v - R_w)(1)^2 = (0.405 - 0.375)(1)^2 = 0.030 \text{ in}^3$$

$$V_w = (4)(2)(100)\ \frac{\pi}{4}\ (0.0045)^2 = 0.01272 \text{ in}^3$$

$$\varepsilon = \frac{V_t - V_w}{V_t} = \frac{0.030 - 0.01272}{0.030} = 0.58$$

d. Wire Cloth Stacking Factor

A stacking factor, S, will be defined as the average layer thickness divided by the wire diameter. This will be determined for the 100 mesh wire cloth and then used in calculations for other mesh size plain weave wire cloth which is to be installed in the same manner.

From the 100 mesh wick

$$\text{Average wick thickness} = \frac{R_v - R_w}{4} = \frac{0.405 - 0.375}{4} = 0.00775"$$

$$S = \frac{0.00775}{0.0045} = 1.72$$

e. Optimum Wick Parameters

Calculated for water at 15.0" Hg vacuum where:

$T_{sat} = 179.14°F$

$\rho_v = 0.01955\ lb_m/ft^3$

$\rho_\ell = 61.48\ lb_m/ft^3$

$\gamma = 0.00427\ lb/ft$

$\mu = 0.726 \times 10^{-5}\ lb\text{-}sec/ft^2$

$L = 990.7\ Btu/lb_m$

and assuming

$$\frac{b}{\varepsilon} = 20.0$$

$\theta = 0°$

(1) Maximum Power

Using equation (11)

$$(Q_{max})_{opt} = \frac{4\pi R_w^2 L}{3}\left[\frac{2\rho_v\rho_\ell\varepsilon\gamma^2\cos^2\theta}{(\pi^2-4)bZ\mu}\right]^{1/3}$$

$$(Q_{max})_{opt} = \frac{4\pi(0.03125)^2(990.7)}{3(9.4799 \times 10^{-4})} \cdot \left[\frac{2(0.01955)(61.48)(0.00427)^2(1)(32.17)}{(\pi^2-4)(20.0)(1.166)(0.726 \times 10^{-5})}\right]^{1/3}$$

$$(Q_{max})_{opt} = 4804 \text{ watts}$$

(2) Capillary Radius

Using equation (10)

$$(r_c)_{opt} = \frac{b\mu Z\ Q_{max}}{4\pi(R_w^2-R_v^2)\rho_\ell L\gamma\ \cos\theta}$$

and equation (9)

$$R_v^2 = \frac{2}{3} R_w^2$$

$$\therefore \quad (r_c)_{opt} = \frac{3b\mu ZQ}{4\pi R_w^2 \rho_\ell \varepsilon L\gamma}$$

$$(r_c)_{opt} = \frac{3(20)(0.726 \times 10^{-5})(1.166)(4804)(9.4799 \times 10^{-4})}{4\pi(0.03125)^2(61.48)(990.7)(0.00427)}$$

$$(r_c)_{opt} = 0.000725' = 0.0087"$$

(3) Mesh Size

Considering 35 mesh market grade wire cloth, $d_w = 0.011"$

$$r_c = \frac{1}{2M} - r_w$$

$$r_c = \frac{1}{2(35)} - \frac{0.011}{2} = 0.00878"$$

(4) Wick Thickness

Using equation (9)

$$R_v = 0.816\ R_w = (0.816)(0.375) = 0.306"$$

$$\text{Thickness} = R_w - R_v = 0.375" - 0.306" = 0.069"$$

$$\text{Layers} = \frac{R_w - R_v}{d_w S}$$

$$\text{Layers} = \frac{0.069}{(0.011)(1.72)} = 3.64 \text{ or } 4 \text{ layers}$$

f. Critical Superheat

Using equation (8) with $r_n = r_c$

$$T_w - T_{sat} = \frac{2\gamma T_{sat}}{L\rho_v r_n}, \quad \text{where } T_{sat} \text{ is absolute temperature}$$

$$T_w - T_{sat} = \frac{2(0.00427)(460 + 179.14)}{(990.7)(0.01955)(0.000229)(778)} = 1.582\ °F$$

g. Maximum Power

Using equation (14)

$$AQ^2 + BQ - C = 0 \quad \text{with} \quad \theta = 0$$

where

$$A = \frac{(1-4/\pi^2)}{8\rho_v R_v^4 L^2} = \frac{(1-4/\pi^2)}{(8)(0.01955)(0.03375)^4(990.7)^2(32.17)}$$

$$= 0.17871\ \frac{\text{lb-sec}^2}{\text{ft}^2\text{-Btu}^2}$$

$$B = \frac{b\mu Z}{2\pi(R_v^2 - R_w^2)\rho_\ell \varepsilon r_c^2 L}$$

$$= \frac{(25)(0.726 \times 10^{-5})(1.166)}{2\pi(0.03375^2 - 0.03125^2)(61.48)(0.000229)^2(990.7)}$$

$$B = 62.614 \text{ lb-sec/ft}^2\text{-Btu}$$

$$C = \frac{2\gamma \cos\theta}{r_c} = \frac{2(0.00427)(1)}{0.000229} = 37.196 \frac{\text{lb}}{\text{ft}^2}$$

$$0.178711Q^2 + 62.614\ Q - 37.196 = 0$$

Disregarding the first term the approximate

$$Q_{max} = 0.59405 \frac{\text{Btu}}{\text{sec}}$$

And by iteration the actual $Q_{max} = 0.59305 \frac{\text{Btu}}{\text{sec}}$

$$\text{Error in approximation} = \frac{(0.59405 - 0.59305)(100)}{0.59305}$$

$$= 0.168\%$$

h. Effective Wick Conductivity

Using equation (4) for water at 15.0" Hg

$$k_{eff} = \varepsilon k_\ell + (1 - \varepsilon)\ k_w$$

and $k_w = 0.25\ k_{ss}$

$$k_{eff} = (0.58)(0.39) + (1-0.58)(10.0)(0.25) = 1.276 \frac{\text{Btu}}{\text{ft-hr-°F}}$$

i. Effective Wick Thickness

Using equations (12) and (13) at 50 watts

$$R_v' = R_w \exp\left[\frac{k_{eff} A(T_w - T_{sat})}{R_w Q}\right]$$

$$R_v' = R_w \exp\left[\frac{(1.276)\ (0.00695)\ (4.50)}{(0.03125)(50)(3.412)}\right] = 0.4042"$$

$$d = R_v' - R_w = 0.4042" - 0.375" = 0.0292"$$

j. Dynamic Response Time Constant

Using an exponential relation for the increasing pressure case in Figure 18,

$$\frac{T_\tau - T_f}{T_o - T_f} = e^{-\frac{t}{\tau}}$$

$$T_\tau = (228 - 169)(0.632) + 169 = 206°F$$

$\therefore$ τ = 55 seconds from Figure 18.

APPENDIX B

ERROR ANALYSIS

DISCUSSION

Uncertainties in the various measurements in the experiment cause uncertainties in the results. Some uncertainties which have an effect on this apparatus include the relative inaccuracy in pressure measurement using a bourdon-tube type gage at low pressures, not knowing exact atmospheric pressure in the immediate vicinity of the gage, thermocouple deviation from standard, electrical power fluctuation, instrument errors, and uncertainties in reading the last significant figure on instrument dials.

An attempt is made to evaluate a 0.95 probability uncertainty interval for these input uncertainties and then propagate through the calculations to determine the expected error in results, again with a 0.95 probability interval. A square-sum-root procedure is generally used in this error analysis. Sample calculations shown are for determining maximum heat transfer rate as a function of pressure.

INPUT UNCERTAINTIES

Mesh size, $M = 100 \pm 1$ (0.95 uncertainty interval)

Mesh wire radius, $r_w = 0.0045 \pm 0.0001"$

Wick radius, $R_w = 0.374 \pm 0.001"$

Effective vapor radius, $R_v' = 0.390 \pm 0.005"$

Based on water at 15.0" Hg

Saturation Pressure, $p = 15.0 \pm 0.5$" Hg

Saturation Temperature, $T_{sat} = 179.14° \pm 1.5°F$

$$N = 303.15 \pm 2.06 \ \frac{\text{Btu-hr-lb}_f}{\text{ft}^3 - \text{lb}_m}$$

Power Input, $Q_{obs} \pm 10$ watts

Thermocouples ± 0.75 °F

SAMPLE CALCULATION

$$r_c = \frac{1}{2M} - r_w \qquad \text{equation (3)}$$

$$\frac{\delta r_c}{r_c} = \left[\left(\frac{\delta M}{M}\right)^2 + \left(\frac{\delta r_w}{r_w}\right)^2 \right]^{1/2}$$

$$\frac{\delta r_c}{r_c} = \left[\left(\frac{1}{100}\right)^2 + \left(\frac{0.0001}{0.0045}\right)^2 \right]^{1/2} = 0.0244$$

Equation (15)

$$Q_{max} = \frac{4\pi (R_v'^2 - R_w^2) \varepsilon r_c}{bZ} \ N \cos \theta$$

And $\frac{b}{\varepsilon}$, Z, cos θ have been selected so that the equation fits through a given point which thus fixes these quantities.

$$\therefore \left(\frac{\delta Q}{Q}\right)_{max} = \left[\left(\frac{2\delta R_v'}{R_v'}\right)^2 + \left(\frac{2\delta R_w}{R_w}\right)^2 + \left(\frac{\delta r_c}{r_c}\right)^2 + \left(\frac{\delta N}{N}\right)^2 \right]^{1/2}$$

$$\left(\frac{\delta Q}{Q}\right)_{max} = \left\{ \left[\frac{2(0.005)}{0.390}\right]^2 + \left[\frac{2(0.001)}{0.374}\right]^2 + 0.0244^2 + \left(\frac{2.06}{303.15}\right)^2 \right\}^{1/2}$$

$$\left(\frac{\delta Q}{Q}\right)_{max} = 0.036417$$

$$\delta Q_{max} = (0.036417)(360) = 13.11 \text{ watts}$$

INITIAL DISTRIBUTION LIST

		No. Copies
1.	Defense Documentation Center Cameron Station Alexandria, Virginia 22314	20
2.	Library Naval Postgraduate School Monterey, California 93940	2
3.	Naval Ship Systems Command (Code 2052) Navy Department Washington, D. C. 20360	1
4.	Mechanical Engineering Department Naval Postgraduate School Monterey, California 93940	2
5.	Professor P. J. Marto Mechanical Engineering Department Naval Postgraduate School Monterey, California 93940	4
6.	Professor P. F. Pucci Mechanical Engineering Department Naval Postgraduate School Monterey, California 93940	1
7.	LT. W. L. Mosteller, USN Fleet Activities, Sasebo c/o Fleet Post Office Seattle, Washington 98766	4

DOCUMENT CONTROL DATA - R&D

(Security classification of title, body of abstract and indexing annotation must be entered when the overall report is classified)

1. ORIGINATING ACTIVITY *(Corporate author)*
Naval Postgraduate School
Monterey, California 93940

2a. REPORT SECURITY CLASSIFICATION
UNCLASSIFIED

2b GROUP

3. REPORT TITLE
THE EFFECT OF NUCLEATE BOILING
ON HEAT PIPE OPERATION

4. DESCRIPTIVE NOTES *(Type of report and inclusive dates)*
Masters Thesis, April 1969

5. AUTHOR(S) *(Last name, first name, initial)*
William Leidy Mosteller, Lieutenant, USN

6. REPORT DATE	7a. TOTAL NO. OF PAGES	7b. NO. OF REFS
April 1969	92	15

8a. CONTRACT OR GRANT NO.

b. PROJECT NO.

c.

d.

9a. ORIGINATOR'S REPORT NUMBER(S)

9b. OTHER REPORT NO(S) *(Any other numbers that may be assigned this report)*

10. AVAILABILITY/LIMITATION NOTICES
Distribution of this document is unlimited.

11. SUPPLEMENTARY NOTES

12. SPONSORING MILITARY ACTIVITY
Naval Postgraduate School
Monterey, California 93940

13. ABSTRACT

An everted experimental stainless steel heat pipe was designed and operated to observe nucleate boiling in the wick and to determine the effects of such boiling on the overall operation of the pipe. Four layers of 100 mesh stainless steel wire cloth were used as the wick structure and both water and ethyl alcohol were used as working fluids. A pressure adjusting system was included so that observations could be made as a function of internal vapor pressure.

A type of boiling was observed which did not appear to affect the overall operation of the pipe and was detectable only by visual observation. The pipe operated in a regime dominated by high liquid flow resistance. Observations indicated effective values for the pipe length, wetted wick thickness, and contact angle. With these modifications, maximum heat transfer rates were in reasonably close agreement with theory.

The pressure adjuster provided a means of easily controlling the operating conditions of the heat pipe. Heat could be removed from a constant power source at any desired temperature within the limitations of the system.

DD FORM 1 JAN 64 1473

14 KEY WORDS	LINK A		LINK B		LINK C	
	ROLE	WT	ROLE	WT	ROLE	WT
HEAT PIPE						
CONTROLLABLE HEAT PIPE						
NUCLEATE BOILING						
HEAT TRANSFER						
WICK						